ORBITAL ANGULAR MOMENTUM OF PARTIALLY COHERENT BEAMS THROUGH ATMOSPHERIC TURBULENCE

by

Arash Shiri

A dissertation submitted to the faculty of
The University of North Carolina at Charlotte
in partial fulfillment of the requirements
for the degree of Doctor of Philosophy in
Optical Science and Engineering

Charlotte

2024

Approved by:

Dr. Greg Gbur

Dr. Glenn Boreman

Dr. Tom Suleski

Dr. Arindam Mukherjee

ABSTRACT

ARASH SHIRI. Orbital Angular Momentum of Partially Coherent Beams Through Atmospheric Turbulence. (Under the direction of DR. GREG GBUR)

The orbital angular momentum of light is a promising candidate as an information carrier in optical communication systems to enhance the capacity of data channels. However, the effects of atmospheric turbulence significantly degrade the quality of light beams, thereby imposing limitations on the range of reliable data transmission. To address this issue, researchers have been actively seeking methods to enhance the resilience of light against fluctuations of refractive index due to the atmospheric turbulence. It has long been recognized that partially coherent beams exhibit greater robustness in propagation through turbulence. Consequently, transitioning from full coherence to partial coherence has been suggested as a solution. Conversely, in OAM-based communications, reducing coherence results in broadening of the OAM spectrum, thus increasing cross-talk between adjacent channels. Therefore, utilizing partially coherent beams in free space communications entails both benefits and drawbacks.

The main objective of this dissertation is to explore various classes of partially coherent beams through analytical approaches in order to identify a robust OAM spectrum in the presence of atmospheric turbulence. The results are presented in three different articles. The first article introduces a simplified version of the extended Huygens-Fresnel principle which is a widely used method of turbulence propagation. The discoveries outlined in the first article substantially alleviate the mathematical complexity associated with propagation in random media, thereby enabling analytical exploration of the propagation of partially coherent beams in random media. The second article presents an optimization criterion associated with a specific class of partially coherent beams, substantially enhancing their resistance against turbulence.

Finally, the third article thoroughly investigates the behavior of three categories of partially coherent beams in interaction with atmosphere, providing a detailed comparison of their respective resistance. The compilation of these three articles presents a comprehensive study of the impact of atmospheric fluctuations on the orbital angular momentum spectrum of partially coherent beams.

TABLE OF CONTENTS

LIST OF FIGURES

LIST OF ABBREVIATIONS

CCB Circularly Coherent Beam

CCVB Circularly Coherent Vortex Beam

CSD Cross Spectral Density

DOC Degree of Coherence

eHF extended Huygens-Fresnel

GSM Gaussian-Schell Model

OAM Orbital Angular Momentum

PCB Partially Coherent Beam

PCVB Partially Coherent Vortex Beam

RMS Root Mean Square

SD Standard Deviation

tGSM twisted Gaussian-Schell Model

CHAPTER 1: INTRODUCTION

Structured light refers to light fields characterized by nontrivial phase, polarization, and coherence [1]. Recently, it has been demonstrated that structured light holds significant potential for enhancing a variety of optical applications [2, 3]. Orbital angular momentum (OAM) represents a distinct aspect associated with the phase pattern of light, which can be understood as the twist of the helical phase front. In optical communications, leveraging OAM can substantially increase data channel capacity [4, 5]. Since the OAM modes existing in a light field establish orthogonal states, each mode can function as a separate data channel. Thus, OAM can be regarded as an additional degree of freedom, alongside other light properties such as wavelength, polarization, and phase, capable of transmitting data within a single signal.

However, in free space propagation, the fluctuations in the refractive index of the medium caused by atmospheric turbulence degrade the quality of optical beams. To address this issue, researchers have dedicated significant effort to finding methods to enhance the beam's resilience against these detrimental turbulence effects. A demonstrated result of these endeavors is that the beams with partial coherence exhibit higher resistance than a fully coherent beam [6, 7, 8]. Hence, reducing the coherence of light beams at their source can serve as a method to improve the reliability of data transmission in free space. On the other hand, in OAM-based optical communications, reducing coherence leads to the redistribution of energy among OAM modes, consequently increasing the likelihood of cross-talk between adjacent data channels, as each channel corresponds to a distinct OAM mode. With that being said, transitioning from perfect coherence to partial coherence can bring about both advantages and disadvantages, signifying the importance of analytical details of optimization of

the OAM spectrum of PCBs in interaction with random media. These optimization attempts run into challenges due to the complicated nature of turbulence. Applying simulation approaches to study the PCBs in turbulence often requires employing the multiple phase screen method, which can be time-consuming and challenging to optimize since the underlying physics of the interaction remain hidden within the simulations [9]. The conventional analytical method for describing wave propagation through turbulence is the extended Huygens-Fresnel (eHF) principle [10]. In this approach, turbulence effects are incorporated as a complex phase that depends on the correlation of beams at various points on the source and detector plane. However, evaluating the integrals associated with the eHF principle is exceedingly complex, and in nearly all cases, finding an analytic solution is not feasible.

Hence, the initial step in an analytical study of PCB propagation through turbulence should be identifying a simplified approach. To achieve this, the first article of this dissertation presents a modified version of the eHF method for wave propagation. In this modification, the four-fold integral of the standard eHF principle is simplified to a two-fold integral. This simplification allowed us to explore the behavior of different classes of PCBs in random media and examine the impact of various parameters of the source on the robustness of the corresponding OAM spectrum.

The preparation of a light beam with partial coherence entails randomizing a characteristic parameter of the fully coherent beam at its source such as phase, beam axis position, and radius of curvature. Various classes of PCBs are associated with different methods of randomization applied to the coherent fields, resulting in different distributions of OAM in the field cross section. In this study, the three different classes that are investigated are: 1- Rankine model beam which is characterized by probabilistically determining the position of the beam axis. Via randomizing the beam axis position of a Gaussian vortex beam, the reduction in spatial coherence appears as a Schell model term in the beam expression. 2- Twisted Gaussian-Schell

model beam in which the spatial coherence is reduced by introducing a twist phase to the Gaussian beam, in addition to decreasing the effective correlation width through the Schell model structure. In this type of PCB, the OAM is induced by the twist phase. 3- Circularly Coherent Beam (CCB) which is defined as a partially coherent source composed of the superposition of a finite number of beams with various radii of curvature. The resulting self-focusing beam will exhibit full coherence in the azimuthal direction, while being partially coherent in the radial direction, which is known as circular coherence.

The introduced modified eHF method is employed to investigate the behavior of PCBs interacting with turbulence. Examining the free space propagation of the mentioned three types of PCBs through turbulence and analyzing the behavior of their respective OAM spectrum under the influence of both atmospheric effects and coherence reduction, it was observed that, in short propagation distances, the disadvantages of reducing coherence of the source, such as the spreading of the OAM spectrum, outweigh its benefits, namely enhancing the beam's stability against refractive index fluctuations. However, by extending the propagation to longer distances, the pre-randomized Rankine model and twisted Gaussian-Schell model beams exhibit significantly higher stability compared to the coherent beam.

In the process of generating a partially coherent beam with circular coherence, which is achieved by linearly combining Gaussian beams with various radii of curvature, a specific optimization approach can be introduced. This approach entails modulating the beam parameters at the source in such a manner that the robustness of its OAM spectrum surpasses that of its fully coherent counterpart, only for propagation up to a particular distance. In our calculations, a criterion is established by introducing a parameter that allows us to estimate the selection of the range of radii of curvature defining the superimposed beams. In other words, for a particular propagation distance through turbulence, achieving resistance in the OAM spectrum

is accomplished by selecting an appropriate focal distance associated with the combination of several self-focusing beams.

In chapter 2 of this dissertation, the modified eHF method for turbulence propagation is presented in detail. In this article two criteria introduced to roughly estimate the intensity and coherence resistance of PCBs through atmospheric turbulence.The accuracy of these criteria is assessed by propagating a Gaussian-Schell model beam through turbulence. The results demonstrate that the introduced parameters effectively approximate the resistance distance for both the intensity and coherence of light.

Chapter 3 outlines the concept of CCB, introduces the method of generating it at the source, and discusses the optimization technique for propagating it through turbulence with a stable OAM spectrum.

In chapter 4, the behavior of all three types of PCBs in propagation through atmospheric turbulence is analyzed and compared. The cross spectral density (CSD) corresponding to each PCB is evaluated in propagation in free space and through turbulence. The findings suggest that the optimal choice of beam type for efficient data transmission in free space is contingent upon various factors, including beam size at the source, propagation distance, and turbulence strength. Considering these influential factors, we can accordingly design a partially coherent source of OAM light, which demonstrates greater reliability compared to a fully coherent source in optical communications.

CHAPTER 2: MODIFIED HUYGENS-FRESNEL METHOD FOR PROPAGATION OF PARTIALLY COHERENT BEAMS THROUGH TURBULENCE

2.1 Abstract

Partially coherent beams (PCBs) have been extensively studied as a method to mitigate the deleterious effects of atmospheric turbulence for applications such as free space optical communication. However, it can be difficult to study and assess the performance of PCBs in turbulence due to the complicated physics of the atmosphere and the wide variety of partially coherent beams possible. Here, we introduce a modified approach to study the propagation of second order field moments of PCBs analytically in turbulence, reformulating the problem in terms of free-space propagation of the beam. We illustrate the method by studying a Gaussian Schell-model beam in turbulence.

2.2 Introduction

In recent years, there has been an explosion of interest in the use of structured light – light possessing nontrivial phase, polarization and coherence properties – to improve a variety of optical applications [1, 2]. In particular, there has been intense research on the use of the orbital angular momentum (OAM) of light as the information carrier in free space optical communications in order to increase the channel capacity [3, 4, 5].

However, atmospheric turbulence inevitably degrades the quality of all optical beams, limiting the useful range of free space applications; this is even more of a concern for OAM beams, as the OAM is carried in the phase structure of light. It has long been known that partially coherent beams (PCBs) are more resistant to atmo-

spheric turbulence [6, 7, 8], as they are in a sense "pre-randomized," and researchers have put much effort into understanding and optimizing the coherence properties of light for various applications in random media [9, 10]. Such optimization efforts are challenging, due to the complicated nature of turbulence. Simulations of PCBs in turbulence can be done using a multiple phase screen method [11, 12], but such an approach is time-consuming and difficult to optimize, because the physics of the interaction is hidden in the simulations. The traditional analytical method for studying the effects of turbulence is the extended Huygens-Fresnel (eHF) method, in which the field from the source plane is propagated to the detector plane in the form of turbulence-perturbed spherical waves [13, 14]. This method requires the evaluation of a four-fold integral, making it difficult to evaluate even when a simplified model of turbulence is used. Furthermore, the complexity of the integral again makes it difficult to determine how to optimize coherence for atmospheric work.

Because of these difficulties, several attempts have been made over the years to approach the analytic propagation problem differently. In 2007, Gbur and Korotkova [15] rederived the extended Huygens-Fresnel method using a plane wave basis instead of a spherical wave basis, getting results that are mathematically very similar to the original. In 2016, Wang and Korotkova introduced a convolution approach for beam propagation in random media [16], finding the spectral density to be a double convolution of three functions.

In this paper, we take a different approach for analyzing the analytic propagation of a partially coherent field through atmospheric turbulence. Using Fresnel transforms, the extended Huygens-Fresnel method is reformulated and the propagation is instead represented as the perturbation of the PCB propagating through free space. When a simplified model of turbulence is used, this new approach gives a clearer physical picture of the effects of turbulence on the propagated field. We illustrate the use of this method by applying it to the traditional class of Gaussian Schell-model beams

propagating through the atmosphere.

We begin by reviewing the extended Huygens-Fresnel method, then introduce our modification of it. We then look at how the method simplifies with approximate models of turbulence, and then consider the example of Gaussian Schell-model beams. We show that the modified Huygens-Fresnel method provides several length scales for estimating the turbulence resistance of a partially coherent beam to second-order.

2.3 The Extended Huygens-Fresnel Method

The extended Huygens-Fresnel principle is built upon the traditional Huygens-Fresnel principle and involves the integral [14],

$$U(\mathbf{r}, z) = -\frac{ik}{2\pi z} \exp(ikz) \iint_{-\infty}^{\infty} d^2\rho \, U_0(\boldsymbol{\rho}, 0) \exp\left[\frac{ik}{2z} |\mathbf{r} - \boldsymbol{\rho}|^2 + \Psi(\mathbf{r}, \boldsymbol{\rho})\right], \tag{2.1}$$

where U_0 is the field at the source, $k = 2\pi/\lambda$ is the wave number and $\boldsymbol{\rho}$ and $\mathbf{r}$ are position vectors in the source and output transverse planes, respectively. The quantity $\Psi(\mathbf{r}, \boldsymbol{\rho})$ denotes the complex phase perturbation of the spherical wave originating at $\boldsymbol{\rho}$ and measured at $\mathbf{r}$ due to refractive index fluctuations, as determined using the first Rytov approximation. The properties of this phase perturbation will be discussed momentarily.

The first-order moment of the field averages to zero, so we turn to the second-order moment, or the cross-spectral density of the field. We begin by assuming a coherent quasi-monochromatic source field and look at the average over an ensemble of turbulence realizations. We define the output cross-spectral density as

$$W(\mathbf{r}_1, \mathbf{r}_2; \omega) = \left\langle U^*(\mathbf{r}_1, \omega) U(\mathbf{r}_2, \omega) \right\rangle_T, \tag{2.2}$$

where $\langle \cdots \rangle_T$ represents the average over the turbulence ensemble, and ω represents

the mean frequency. Substituting from Eq. (2.1) into Eq. (2.2), we have

$$\begin{aligned} W(\mathbf{r}_1,\mathbf{r}_2;\omega) = \left(\frac{k}{2\pi z}\right)^2 \iint_{-\infty}^{\infty} d^2\rho_1 \iint_{-\infty}^{\infty} d^2\rho_2\, U_0^*(\boldsymbol{\rho}_1,\omega) U_0(\boldsymbol{\rho}_2,\omega) \\ \times \exp\left\{-\frac{ik}{2z}\Big[\,|\mathbf{r}_1-\boldsymbol{\rho}_1|^2 - |\mathbf{r}_2-\boldsymbol{\rho}_2|^2\,\Big]\right\} \\ \times \Big\langle \exp\left[\Psi^*(\boldsymbol{\rho}_1,\mathbf{r}_1)+\Psi(\boldsymbol{\rho}_2,\mathbf{r}_2)\right]\Big\rangle_T. \end{aligned} \tag{2.3}$$

If we consider a source that is already partially coherent, then it has its own independent ensemble, and we may write

$$W_0(\boldsymbol{\rho}_1,\boldsymbol{\rho}_2;\omega) = \big\langle U_0^*(\boldsymbol{\rho}_1,\omega) U_0(\boldsymbol{\rho}_2,\omega)\big\rangle_\omega, \tag{2.4}$$

where $\langle\cdots\rangle_\omega$ represents an average over an ensemble of monochromatic realizations of the field, as first introduced by Wolf [17]. For a quasi-monochromatic field, the cross-spectral density at frequency ω is a good approximation to the properties of the field as a whole. It should be noted that the ensemble of the source is independent of the ensemble of the turbulence; then the cross-spectral density of a partially coherent field at the detector plane is given by

$$\begin{aligned} W(\mathbf{r}_1,\mathbf{r}_2;\omega) = \left(\frac{k}{2\pi z}\right)^2 \iint_{-\infty}^{\infty} d^2\rho_1 \iint_{-\infty}^{\infty} d^2\rho_2\, W_0(\mathbf{r}_1,\mathbf{r}_2;\omega) \\ \times \exp\left\{-\frac{ik}{2z}\Big[\,|\mathbf{r}_1-\boldsymbol{\rho}_1|^2 - |\mathbf{r}_2-\boldsymbol{\rho}_2|^2\,\Big]\right\} F(\mathbf{r}_1,\mathbf{r}_2;\boldsymbol{\rho}_1,\boldsymbol{\rho}_2), \end{aligned} \tag{2.5}$$

where we have introduced the turbulence function

$$F(\mathbf{r}_1,\mathbf{r}_2;\boldsymbol{\rho}_1,\boldsymbol{\rho}_2) \equiv \Big\langle \exp\left\{\Psi^*(\boldsymbol{\rho}_1,\mathbf{r}_1)+\Psi(\boldsymbol{\rho}_2,\mathbf{r}_2)\right\}\Big\rangle_T \tag{2.6}$$

for brevity. Using the method of cumulants [18] limited to first and second orders, the function $F(\mathbf{r}_1,\mathbf{r}_2;\boldsymbol{\rho}_1,\boldsymbol{\rho}_2)$ may be determined for homogeneous and isotropic tur-

bulence and is of the form [14],

$$\begin{aligned}&\left\langle \exp\left[\Psi(\boldsymbol{\rho}_1,\mathbf{r}_1)+\Psi^*(\boldsymbol{\rho}_2,\mathbf{r}_2)\right]\right\rangle \\ &= \exp\left\{-4\pi^2k^2z\int_0^1 d\xi\int_0^\infty d\kappa\,\kappa\Phi_n(\kappa)\Big\{1-J_0\left[|(\xi-1)\boldsymbol{\rho}-\xi\mathbf{r}|\,\kappa\right]\Big\}\right\},\end{aligned} \tag{2.7}$$

where $\mathbf{r}=\mathbf{r}_2-\mathbf{r}_1$ and $\boldsymbol{\rho}=\boldsymbol{\rho}_2-\boldsymbol{\rho}_1$ are the difference vectors at the detector and source planes, respectively, $\xi = z/L$ is a unitless integration parameter, J_0 is the Bessel function of zero order and $\Phi_n(\kappa)$ is the spatial power spectrum of the turbulence. It is important to note that this function only depends on the difference vectors, and may be written as

$$F(\mathbf{r}_1,\mathbf{r}_2;\boldsymbol{\rho}_1,\boldsymbol{\rho}_2)=F(\mathbf{r},\boldsymbol{\rho}). \tag{2.8}$$

From Eq. (2.5), we see that determining the cross-spectral density in the detector plane involves a four-fold integral. These integrals are non-separable, due to the correlations in the turbulence and the source cross-spectral density. With approximations for the turbulence function and certain classes of sources, it is possible to evaluate this integral analytically; however, the results are complicated and generally give little insight into why one PCB may work better than another. Due to the large variety of structured PCBs possible – see, for example, Refs. [19] and [20] – such an approach is not ideal. In the next section, we introduce our modified Huygens-Fresnel method to improve upon these limitations.

2.4 The Modified Huygens-Fresnel Method

Returning to Eq. (2.5), we note that the free-space Huygens-Fresnel kernels, e.g. $\exp[ik(\mathbf{r}-\boldsymbol{\rho})^2/2z]$, remain unaltered in the equation. This suggests that we attempt to simplify the equation by writing the source cross-spectral density in terms of its

inverse Fresnel transform, i.e.

$$W_0(\boldsymbol{\rho}_1, \boldsymbol{\rho}_2) = \left(\frac{k}{2\pi z}\right)^2 \iint_{-\infty}^{\infty} d^2 r_1' \iint_{-\infty}^{\infty} d^2 r_2' \, \widehat{W}(\mathbf{r}_1', \mathbf{r}_2') \times \exp\left\{\frac{ik}{2z}\left[\,|\mathbf{r}_1' - \boldsymbol{\rho}_1|^2 - |\mathbf{r}_2' - \boldsymbol{\rho}_2|^2\,\right]\right\}. \tag{2.9}$$

Here, $\widehat{W}(\mathbf{r}_1', \mathbf{r}_2')$, the inverse Fresnel transform of $W_0(\boldsymbol{\rho}_1, \boldsymbol{\rho}_2)$, represents the cross-spectral density that would appear at the detector plane at distance z if it had propagated through free space. The geometry of the system and the relevant variables are illustrated in Fig. 2.1.

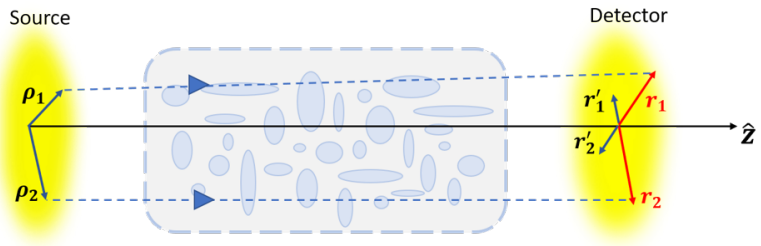

Figure 2.1: Propagation of beam from source ($\boldsymbol{\rho_1}$, $\boldsymbol{\rho_2}$) to detector ($\mathbf{r_1}, \mathbf{r_2}$) through atmospheric turbulence. ($\mathbf{r_1}', \mathbf{r_2}'$) are positions on detector plane receiving the light propagated in free space in the absence of turbulence.

Substituting from Eq. (2.9) into Eq. (2.5) gives

$$W(\mathbf{r}_1, \mathbf{r}_2; \omega) = \left(\frac{k}{2\pi z}\right)^4 \iint_{-\infty}^{\infty} d^2\rho_1 \iint_{-\infty}^{\infty} d^2\rho_2 \iint_{-\infty}^{\infty} d^2 r_1' \iint_{-\infty}^{\infty} d^2 r_2' \, \widehat{W}(\mathbf{r}_1', \mathbf{r}_2') \times \exp\left[\frac{ik}{2z}\left(\,|\mathbf{r}_1' - \boldsymbol{\rho}_1|^2 - |\mathbf{r}_2' - \boldsymbol{\rho}_2|^2 - |\mathbf{r}_1 - \boldsymbol{\rho}_1|^2 + |\mathbf{r}_2 - \boldsymbol{\rho}_2|^2\,\right)\right] F(\mathbf{r}, \boldsymbol{\rho}). \tag{2.10}$$

At first glance, it appears that we have made our calculation even more complicated, as it is now an eight-fold integral. We may simplify it significantly, however, by

converting to sum and difference variables, of the form

$$\begin{aligned} \mathbf{r} =& \mathbf{r}_2 - \mathbf{r}_1 \quad , \quad \mathbf{R} = \frac{\mathbf{r}_2 + \mathbf{r}_1}{2}, \\ \boldsymbol{\rho} =& \boldsymbol{\rho}_2 - \boldsymbol{\rho}_1 \quad , \quad \mathbf{P} = \frac{\boldsymbol{\rho}_2 + \boldsymbol{\rho}_1}{2}, \end{aligned} \tag{2.11}$$

with analogous definitions for $\mathbf{r}'$ and $\mathbf{R}'$. Rewriting Eq. (2.10) in these new variables, we have

$$\begin{aligned} W(\mathbf{r}, \mathbf{R}) = \left(\frac{k}{2\pi z}\right)^4 \iint_{-\infty}^{\infty} d^2 r' \iint_{-\infty}^{\infty} d^2 R' \iint_{-\infty}^{\infty} d^2 \rho \iint_{-\infty}^{\infty} d^2 P \, \widehat{W}(\mathbf{r}', \mathbf{R}') \\ \times \exp\left\{\frac{ik}{2z}\Big[2\mathbf{P}\cdot(\mathbf{r}'-\mathbf{r}) + 2\boldsymbol{\rho}\cdot(\mathbf{R}'-\mathbf{R})\Big]\right\} \\ \times \exp\left[\frac{ik}{2z}\left(3\mathbf{R}\cdot\mathbf{r} - 3\mathbf{R}'\cdot\mathbf{r}'\right)\right] F(\mathbf{r}, \boldsymbol{\rho}). \end{aligned} \tag{2.12}$$

The turbulence function $F(\mathbf{r}, \boldsymbol{\rho})$ is independent of $\mathbf{P}$ due to the homogeneity of the turbulence; this means that we may directly integrate out that variable, resulting in a delta function,

$$\iint d^2 P \, \exp\left[-\frac{ik}{z}\,\mathbf{P}\cdot(\mathbf{r}-\mathbf{r}')\right] = (2\pi)^2 \delta^2\left[\frac{k}{z}(\mathbf{r}-\mathbf{r}')\right]. \tag{2.13}$$

We may then integrate over $\mathbf{r}'$, leaving us with the reduced formula

$$\begin{aligned} W(\mathbf{r}, \mathbf{R}) = \left(\frac{k}{2\pi z}\right)^2 \iint_{-\infty}^{\infty} d^2 R' \iint_{-\infty}^{\infty} d^2 \rho \, \widehat{W}(\mathbf{r}, \mathbf{R}') F(\mathbf{r}, \boldsymbol{\rho}) \\ \times \exp\left\{\frac{ik}{2z}\Big[-3(\mathbf{R}'-\mathbf{R})\cdot\mathbf{r} + 2(\mathbf{R}'-\mathbf{R})\cdot\boldsymbol{\rho}\Big]\right\}. \end{aligned} \tag{2.14}$$

Now the only thing that depends on $\boldsymbol{\rho}$ is the turbulence function $F(\mathbf{r}, \boldsymbol{\rho})$. Defining the Fourier transform of F with respect to $\boldsymbol{\rho}$ as $\tilde{F}(\mathbf{r}, \mathbf{K})$, in the form,

$$\tilde{F}(\mathbf{r}, \mathbf{K}) = \iint_{-\infty}^{\infty} d^2 \rho F(\mathbf{r}, \boldsymbol{\rho}) \exp\left(i\mathbf{K}\cdot\boldsymbol{\rho}\right), \tag{2.15}$$

we may reduce our expression for the cross-spectral density to the form,

$$W(\mathbf{r},\mathbf{R}) = \left(\frac{k}{2\pi z}\right)^2 \iint_{-\infty}^{\infty} d^2R'\ \widehat{W}(\mathbf{r},\mathbf{R}')\tilde{F}\left[\mathbf{r}, \frac{k}{z}(\mathbf{R}'-\mathbf{R})\right] \exp\left[-\frac{3ik}{2z}(\mathbf{R}'-\mathbf{R})\cdot\mathbf{r}\right]. \tag{2.16}$$

Finally, we introduce a new shifted variable $\mathbf{R}'' = \mathbf{R}' - \mathbf{R}$. Our expression becomes

$$W(\mathbf{r},\mathbf{R}) = \left(\frac{k}{2\pi z}\right)^2 \iint_{-\infty}^{\infty} d^2R''\ \widehat{W}(\mathbf{r},\mathbf{R}''+\mathbf{R})\tilde{F}\left(\mathbf{r}, \frac{k}{z}\mathbf{R}''\right) \exp\left(-\frac{3ik}{2z}\mathbf{R}''\cdot\mathbf{r}\right). \tag{2.17}$$

Equation (2.17) is the main result of the paper. It demonstrates that the traditional Huygens-Fresnel method can be reformulated in a way that allows the relevant integrals to be evaluated independently. The free space propagation of the cross-spectral density must be evaluated first; however, this is almost always done anyway to provide a comparison with the behavior of the field in turbulence. The Fourier transform of the turbulence function can be evaluated for simple turbulence models, as we show in the next section. By writing the final result in terms of the shifted variable $\mathbf{R}''$, we can see that the effect of the turbulence on the beam is a form of convolution, in which copies of the free space propagated field are shifted, distorted and overlapped. Further insight into the effects of turbulence will be found in the next section.

2.5 The Quadratic Approximation For The Modified Huygens-Fresnel Method

The turbulence function, given by Eq. (2.7), is generally a function that cannot be readily integrated in either the extended Huygens-Fresnel method or its modification. Though the integrals can be done numerically, one way to simplify them is to use a quadratic approximation for the turbulence function which is a reasonable approximation when the principal effect of turbulence is through tilts in the phase front of the beam [21]; this can be done by approximating the zeroth order Bessel function in

Eq. (2.7) by the first two terms in its Taylor series expansion

$$J_0(x) \approx 1 - x^2 + \ldots, \tag{2.18}$$

as done for example in Ref. [19]. On substituting that into Eq. (2.7), we have

$$F(\mathbf{r}, \boldsymbol{\rho}) = \exp\left[-Q(z)\left(r^2 + \rho^2 + \boldsymbol{\rho} \cdot \mathbf{r}\right)\right], \tag{2.19}$$

where $Q(z)$ is a quantity that characterizes the correlation length of the turbulence, given by

$$Q(z) \equiv \left(\frac{\pi^2 k^2 z}{3}\right) \int_0^\infty d\kappa \left[\, \kappa^3 \, \Phi_n(\kappa) \,\right]. \tag{2.20}$$

and κ is the norm of the two-dimensional spatial frequency in the transverse plane. It is to be noted that an alternative form of the quadratic approximation was introduced by Leader for the weak turbulence case which gives slightly different results [22]; here we restrict our attention to the Taylor series approximation.

To calculate $Q(z)$ in Eq. (2.20) a conventional model for the spatial power spectrum of refractive index fluctuations is used. Among a number of existing models, the Von-Karman model is the one we use going forward, which includes the effects of the inner scale l_0 and outer scale L_0 of turbulence [14],

$$\begin{gathered} \Phi_n(\kappa) = 0.033 C_n^2 \frac{\exp\left(-\kappa^2/\kappa_m^2\right)}{\left(\kappa^2 + \kappa_0^2\right)^{11/6}} \quad , \quad 0 \leq \kappa < \infty. \\ \kappa_m = \frac{5.92}{l_0}, \quad \kappa_0 = \frac{2\pi}{L_0}. \end{gathered} \tag{2.21}$$

The parameter C_n^2 is a measure of turbulence strength and is in the range of $10^{-17} m^{-2/3}$ to $10^{-13} m^{-2/3}$ from the weaker to stronger strengths. We will consider inner and outer scales $l_0 = 2mm$ and $L_0 = 25m$, though in the quadratic approximation

these quantities are essentially averaged out in Eq. (2.20).

With Eq. (2.20), we can now readily evaluate Eq. (2.15) for $\tilde{F}(\mathbf{r}, \mathbf{K})$; the result is of the form

$$\tilde{F}\left(\mathbf{r}, \frac{k}{z}\mathbf{R}''\right) = \frac{\pi}{Q(z)} \exp\left[-\frac{3Q(z)r^2}{4}\right] \exp\left[-\frac{k^2}{4Q(z)z^2}R''^2\right]. \tag{2.22}$$

This expression shows that, within the quadratic approximation, the effect of turbulence on the free-space propagated field is two-fold. First, there is a general loss of spatial coherence as the propagation distance increases, as characterized by the Gaussian function in $\mathbf{r}$. Second, there is an overall wander of the central axis of the beam that depends on the strength of turbulence and the propagation distance; as the beam propagates, the quantity $Q(z)$ increases and so does the wander. Looking back at Eq. (2.17), the complex phase term depending on $\mathbf{R}'' \cdot \mathbf{r}$ is a propagation phase associated with the wander.

This formula gives us a quantitative method of assessing the robustness of a partially coherent beam in atmospheric turbulence, at least to second-order (i.e. to the level of field-field correlations). A robust beam, by definition, will remain largely unchanged by the turbulent atmosphere on propagation; in particular, its spatial coherence will be relatively unperturbed and its intensity profile will be relatively unperturbed. From Eq. (2.22), one expects that the coherence of the PCB will be unperturbed provided its free space value at the detector plane is less than the characteristic length $l(z)$:

$$l(z) = \sqrt{\frac{4}{3Q(z)}}. \tag{2.23}$$

From the same equation, one expects that the intensity profile will be unperturbed provided the beam width is significantly larger than the average wander radius, given by:

$$w(z) = \sqrt{\frac{4Q(z)z^2}{k^2}}. \tag{2.24}$$

This latter observation is in agreement with the early observation that much of the robustness of PCBs in turbulence comes from their greater free-space diffraction [23].

It is to be noted that these two conditions are distinct, suggesting that it may be possible to have a beam with distorted intensity but unperturbed spatial coherence, and vice versa.

We may use these conditions to estimate the robustness of various PCBs in turbulence. It is to be noted that the modified Huygens-Fresnel method can be used both analytically and computationally to evaluate PCBs, as it reduces the four-fold integral of the extended Huygens-Fresnel method to a number of simpler steps.

2.6 Propagation of Gaussian-Schell Model beam in atmospheric turbulence

To test our modified eHF model and the resulting predictions about the effects of a turbulent media on the intensity and degree of coherence of beams, we use the modified eHF model to study the propagation of a partially coherent Gaussian-Schell model beam.

A Schell-model source is characterized by dependence of its coherence only on the difference vector $\boldsymbol{\rho}_1 - \boldsymbol{\rho}_2$, and the cross-spectral density of a Gaussian Schell-model source has the form [24]:

$$W_0(\boldsymbol{\rho}_1, \boldsymbol{\rho}_2) = I_0 \exp\left[-\frac{1}{4\sigma_s^2}(\rho_1^2 + \rho_2^2)\right] \exp\left[-\frac{1}{2\sigma_g^2}|\boldsymbol{\rho}_1 - \boldsymbol{\rho}_2|^2\right], \tag{2.25}$$

where the quantities I_0, σ_s and σ_g are the maximum intensity, the spot size the and correlation width of the beam at the source, respectively.

The first step of applying the modified Huygens-Fresnel method is to find the propagation of the cross-spectral density function in free space using Fresnel propagation.

The result is of the form,

$$\widehat{W}(\mathbf{r}_1', \mathbf{r}_2') = \left(\frac{I_0}{T}\right) \exp\left[-\frac{1}{4\sigma_s'^2}(r_1'^2 + r_2'^2)\right] \exp\left[-\frac{1}{2\sigma_g'^2}|\mathbf{r}_1' - \mathbf{r}_2'|^2\right] \times \exp\left[-\frac{ik}{2R'(z)}(r_1'^2 - r_2'^2)\right]. \tag{2.26}$$

Here $\mathbf{r}_1'$,$\mathbf{r}_2'$ are position vectors on the detector plane and σ_s' and σ_g' are the spot size and correlation width of beam at the detector plane in free space propagation respectively,

$$\sigma_s'^2 = T\sigma_s^2 \quad , \quad \sigma_g'^2 = T\sigma_g^2, \qquad T \equiv 1 + \left(\frac{z}{k\sigma_s}\right)^2 \left(\frac{1}{4\sigma_s^2} + \frac{1}{\sigma_g^2}\right), \tag{2.27}$$

and $R'(z)$ is the radius of curvature of the beam at the detector plane,

$$R'(z) = z\left(\frac{T}{T-1}\right). \tag{2.28}$$

Substituting from these expressions into Eq. (2.17), and using Eq. (2.22) for the turbulence function, the cross-spectral density on propagation through turbulence can be obtained in terms of the position vectors $\mathbf{r}_1$,$\mathbf{r}_2$ in the detector plane,

$$W(\mathbf{r}_1, \mathbf{r}_2) = \left(\frac{I_0}{T+t}\right) \exp\left[-\frac{1}{4\Sigma_s^2}\left(r_1^2 + r_2^2\right)\right] \exp\left[-\frac{1}{2\Sigma_g^2}|\mathbf{r}_1 - \mathbf{r}_2|^2\right] \times \exp\left[-\frac{ik}{2R(z)}(r_1^2 - r_2^2)\right], \tag{2.29}$$

where Σ_s and Σ_g are the spot size and coherence width of the beam at the output plane after turbulence propagation,

$$\Sigma_s^2 = \sigma_s'^2 + \frac{1}{2}w^2(z), \tag{2.30}$$

$$\frac{1}{2\Sigma_g^2} = \frac{1}{2\sigma_g'^2} + \frac{1}{l^2(z)} + \frac{1}{l'^2(z)}. \tag{2.31}$$

The quantities $l(z)$ and $w(z)$ are the characteristic length and average wander radius introduced in previous section, Eqs. (2.23) and (2.24), respectively, and they both depend on the turbulence strength and wavelength of the source. These expressions confirm that, to a rough approximation, the turbulence resistance of the beam profile depends on the relative sizes of σ_s' and $w(z)$, and that the turbulence resistance of the spatial coherence depends on the relative sizes of σ_g' and $l(z)$.

A more refined analysis comes from investigating the parameter $l'(z)$, which depends in a non-trivial way upon the correlation width and spot size of the Gaussian Schell- model beam,

$$\frac{1}{l'^2(z)} = Q(z)\left[\frac{(\frac{z}{k\sigma_s})^2 + (1+T)^2}{T(T+t)}\right] \tag{2.32}$$

where t is given by

$$t = 2Q(z)\left(\frac{z}{k\sigma_s}\right)^2. \tag{2.33}$$

The quantity $R(z)$ in Eq. (2.29) is the average radius of curvature of the beam at the detector plane after propagating in turbulence,

$$R(z) = z\left[\frac{2(T+t)}{T+3t-2}\right]. \tag{2.34}$$

We now consider the turbulence resistance of Gaussian Schell-model beams and whether the simple parameters given earlier are an accurate way of estimating turbulence resistance in this case. According to Eq. (2.30) we can see that the effect of turbulence on intensity is negligible if the ratio

$$\alpha \equiv \frac{\sigma_s'}{w(z)} \tag{2.35}$$

is significantly larger that 1, which is in agreement with the estimate of Eq. (2.24).

Also from Eq. (2.31) coherence of the beam is apparently unperturbed provided that the two ratios

$$\begin{aligned} \beta_1 &\equiv \frac{\sigma_g'}{l(z)}, \\ \beta_2 &\equiv \frac{\sigma_g'}{l'(z)} \end{aligned} \tag{2.36}$$

are significantly smaller that 1. The first of these conditions is analogous to Eq. (2.23), while the second comes from the detailed analysis of a Gaussian Schell-model beam.

In Figure 2.2, the intensity profiles of a Gaussian Schell-model beam on propagation in free space and turbulence are compared, with the source spot size $\sigma_s = 0.5$mm and the source correlation width $\sigma_g = 0.25$mm; because $\sigma_g < \sigma_s$, the source is globally partially coherent. We see that for large values of α, the turbulence effect is negligible and free space and turbulence intensity profiles coincide. As α decreases to values less than 2 over larger propagation distances, the intensity in turbulence begins to diverge from the free space profile and a drop of the peak intensity is observed, which is in agreement with our condition dictated by Eq. (2.24) for an unperturbed intensity.

Figure 2.3 shows similar intensity profiles for $\sigma_s = 0.5$mm and the source correlation width $\sigma_g = 1$m; in this case the field is essentially fully coherent. It can be seen again that the intensity profiles in free space and turbulence begin to diverge when $\alpha < 2$; by comparing the propagation distances in the two figures, we can see that the fully coherent beam shows turbulence effects at significantly shorter distances than the partially coherent beam.

Both figures 2.2 and 2.3 indicate that if the beam size in free space propagation is significantly larger than the average wander parameter defined in Eq.(2.24), regardless of coherence state of the beam, intensity shows higher resistance against atmospheric turbulence.

Figure 2.4(a) shows the degree of coherence (DOC) at the source, in free space

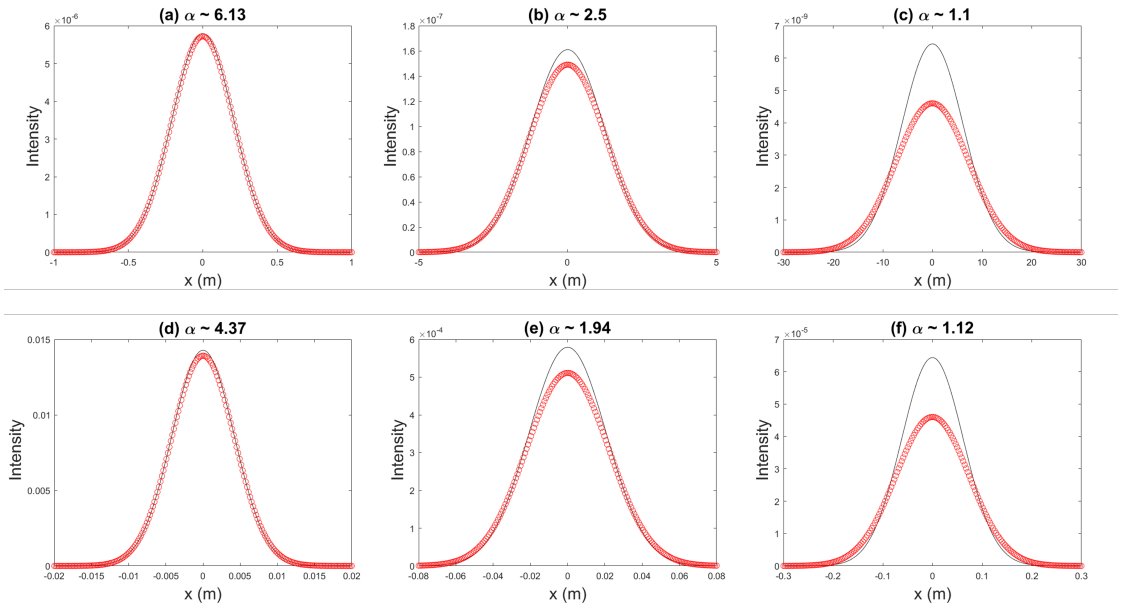

Figure 2.2: Intensity profile of propagation of partially coherent Gaussian-Schell model beam in atmospheric turbulence. Red circles show the turbulence and solid line is the free space intensity profiles. In (a),(b),(c) propagation is through moderate strength turbulence $C_n^2 = 10^{-15}m^{-2/3}$ to distances $0.5km$, $3km$, $15km$ and (d),(e),(f) show propagation through strong turbulence $C_n^2 = 10^{-13}m^{-2/3}$ to distances $10m$, $50m$, $150m$ respectively. Coherence width, spot size and wavelength of source are $0.25mm$, $0.5mm$ and $633nm$ respectively.

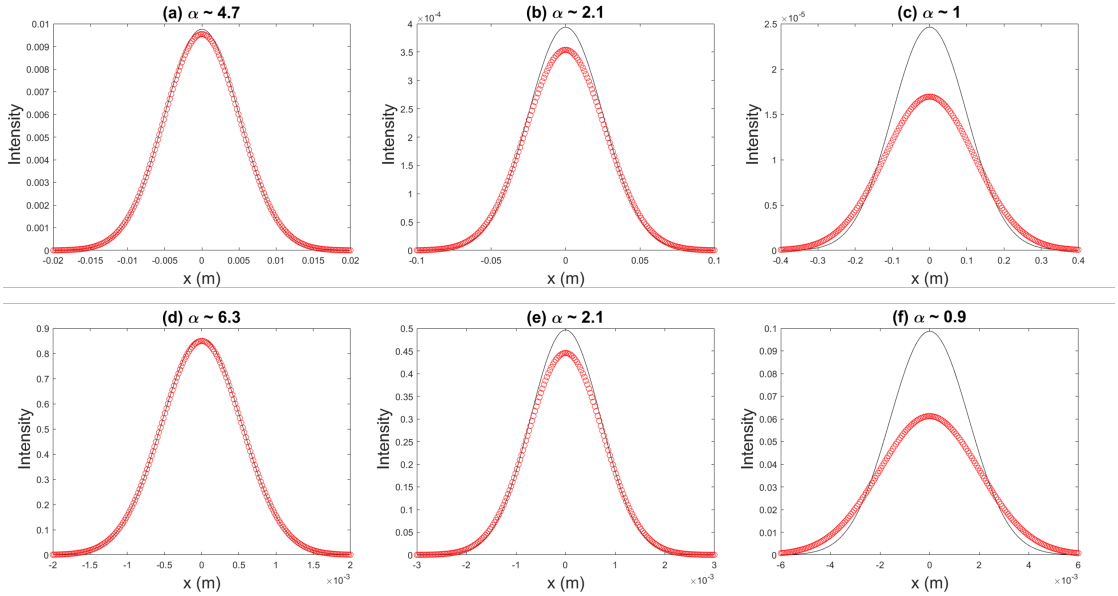

Figure 2.3: Intensity profile of propagation of highly coherent Gaussian-Schell model beam in atmospheric turbulence. Red circles show the turbulence and solid line is the free space intensity profiles. In (a),(b),(c) propagation is through moderate strength turbulence $C_n^2 = 10^{-15}m^{-2/3}$ to distances $50m$, $250m$, $1000m$ and (d),(e),(f) show propagation through strong turbulence $C_n^2 = 10^{-13}m^{-2/3}$ to distances $2m$, $5m$, $15m$ respectively. Coherence width, spot size and wavelength of source are $1m$, $0.5mm$ and $633nm$ respectively.

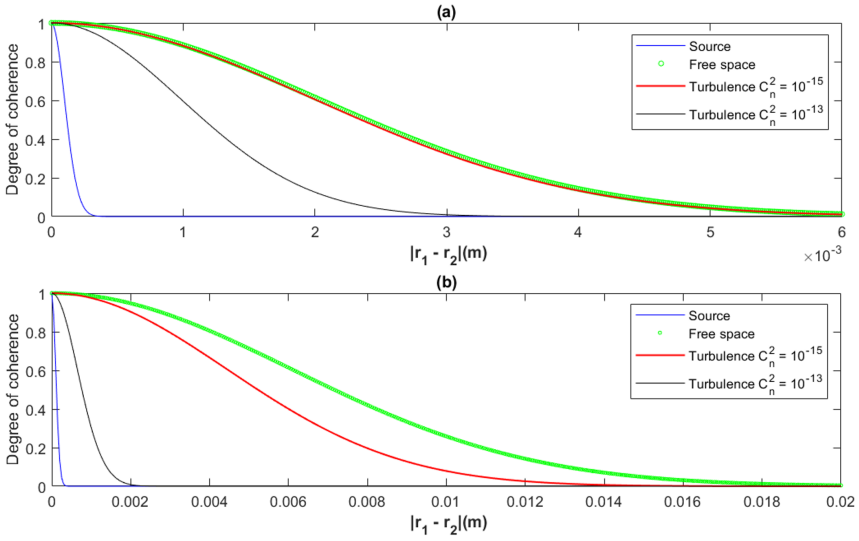

Figure 2.4: DOC of Gaussian-Schell model beam for $z = 10m$(a) and $z = 30m$(b) propagation distances. (a) shows the DOC at the source, detector plane in free space propagation, detector plane through moderate turbulence $C_n^2 = 10^{-15}m^{-2/3}$ with ($\beta_1 \approx 0.08$, $\beta_2 \approx 0.09$), and through strong turbulence $C_n^2 = 10^{-13}m^{-2/3}$ with ($\beta_1 \approx 0.8$, $\beta_2 \approx 1$). In (b) for moderate strength turbulence ($\beta_1 \approx 0.4$, $\beta_2 \approx 0.5$) and for strong turbulence ($\beta_1 \approx 4.3$, $\beta_2 \approx 4.9$). Coherence width, spot size and wavelength of source are $0.1mm$, $0.5mm$ and $633nm$ respectively.

at the detector, and through turbulence at the detector for two distinct turbulence strengths. It can be seen that DOC is indistinguishable from the free space case in moderate strength turbulence; this case satisfies $\beta_1, \beta_2 << 1$.

Figure 2.4(b) shows the same fields over a significantly further propagation distance, and it can be seen that the conditions (2.36) have not been satisfied, and the DOC is significantly lower in turbulence than in free space.

It is to be noted that the spatial coherence degrades over quite short propagation distances in turbulence, at least when compared to the distance over which the intensity profiles show turbulence resistance.

Figure 5 illustrates how the correlation width of the beam evolves in turbulence for various propagation parameters. Over short distances, the correlation width increases on propagation, in accordance with the venerable van Cittert-Zernike theorem, which indicates that spatial coherence generally increases on free-space propagation. At a

critical distance, however, the random phase distortions of the turbulence accumulate to the point that the spatial coherence begins to decrease; the range at which this decay happens is dictated by the conditions of Eq. (2.36). It is of interest to note that, for beams with the same correlation width, the degree of coherence is more turbulence-resistant for larger source beam widths.

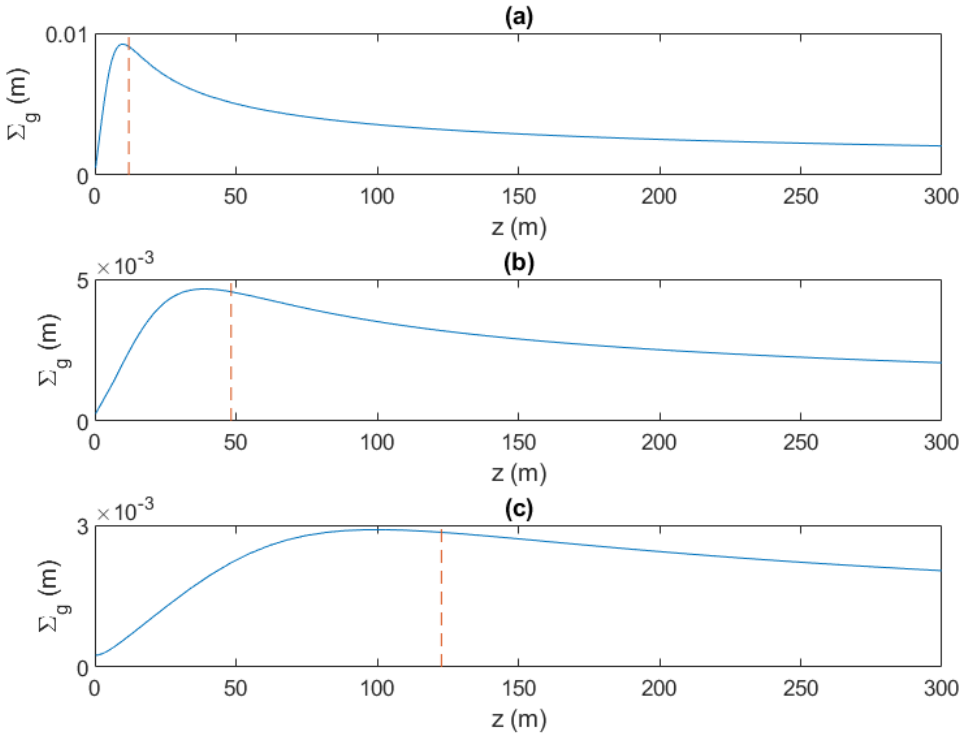

Figure 2.5: Coherence width on the detector plane as a function of propagation distance z through moderate strength turbulence $C_n^2 = 10^{-15} m^{-2/3}$. (a),(b),(c) correspond to sources with beam size $0.25mm$, $0.5mm$ and $2mm$ respectively and the coherence width of the sources is $0.25mm$. The dashed line is the indicator of coherence resistant distance with $\beta_1 \approx 1$.

These examples illustrate that the general conditions dictated by Eqs. (2.23) and (2.24), and their values specific to Gaussian Schell-model beams given by Eqs. (2.35) and (2.36), provide a reasonable estimate of the range of turbulence resistance. These equations have to be solved for the critical z-distance in each case, and it is not immediately obvious how the range of turbulence resistance relates to spatial coherence. In

Figure 2.6, the range of turbulence resistance is plotted as a function of σ_g^{-2}; it can be seen that as spatial coherence decreases, the turbulence resistant distance increases. It is also to be noted that the turbulence resistance increases as the beam width decreases. Smaller beam widths at the source translate into more rapid spreading of the free-space beam on propagation, making them less susceptible to turbulence-induced beam wander.

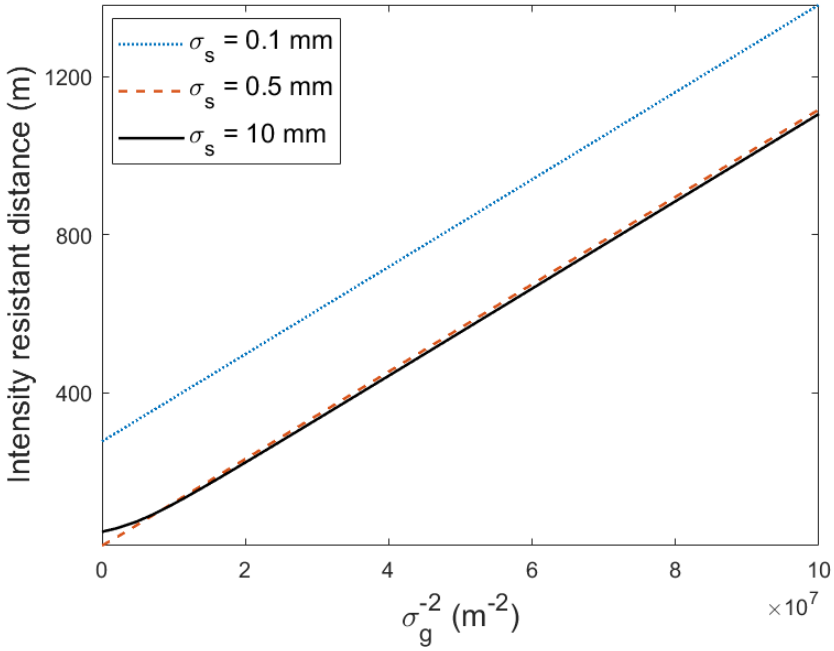

Figure 2.6: Unperturbed intensity propagation distance through strong turbulence $C_n^2 = 10^{-13} m^{-2/3}$ as a function of coherence width of the beam for sources with different beam size.

2.7 Conclusion

We have developed a modified analytic approach for the propagation of partially coherent beams in atmospheric turbulence. In this method, the eHF principle is reformulated so that the effect of turbulence is described as a distortion and wander of the free-space propagated field at the detector. If the binomial approximation is used to simplify the form of the turbulence phase function, the modified eHF principle can be used to estimate the propagation distance over which the intensity profile and

DOC of the field are unaffected by turbulence. Gaussian Schell-model beams were used as an example to test the accuracy of the turbulence resistance estimates, and in this case they were shown to be accurate.

The modified eHF method breaks up the four-fold integral of the traditional eHF method into several steps: the free-space propagation of the field and the wander and distortion of the free-space propagated field at the detector. The free-space propagation of the field is almost always calculated for comparison when studying partially coherent beams in turbulence, so this step doesn't add any significant burden to the calculation. The final integral of the free-space field in turbulence is only two-fold, making it easier to evaluate both analytically and computationally. The results for the beam size of Gaussian Schell-model beams through turbulence is exactly in agreement with Ref. [25] which has used the ordinary eHF principle for propagation.

It is hoped that this technique will make the analysis of various structured PCBs easier to undertake and the results easier to understand. This method only considers the behavior of the fields to second-order (field-field correlations). Considering fourth-order (intensity-intensity) calculations are important in understanding properties like the scintillation of the beams in turbulence and the bit-error rate of free-space optical communication systems, future work will involve studying whether the modified eHF method can be further extended to fourth order.

REFERENCES

[1] O.V. Angelsky, A.Y. Bekshaev, S.G. Hanson, C.Y. Zenkova, I.I. Mokhun and J. Zheng, "Structured Light: Ideas and Concepts," Front. Phys. 8 (2020), 114.

[2] Forbes, A., de Oliveira, M. and Dennis, M.R. Structured light. Nat. Photonics 15 (2021), 253 262.

[3] Y. Ren, Z. Wang, P. Liao, L. Li, G. Xie, H. Huang, Z. Zhao, Y. Yan, N. Ahmed, A. Willner, M. P. J. Lavery, N. Ashrafi, S. Ashrafi, R. Bock, M. Tur, I. B. Djordjevic, M. A. Neifeld, and A. E. Willner, Experimental characterization of a 400 Gbit/s orbital angular momentum multiplexed free-space optical link over 120 m, Opt. Lett. 41(3), 622 625 (2016)

[4] A. E. Willner, Y. Ren, G. Xie, Y. Yan, L. Li, Z. Zhao, J. Wang, M. Tur, A. F. Molisch, and S. Ashrafi, Recent advances in high-capacity free-space optical and radio-frequency communications using orbital angular momentum multiplexing, Philos. Trans. R. Soc., A 375(2087), 20150439 (2017)

[5] X. Yan, L. Guo, M. Cheng, J. Li, Q. Huang, and R. Sun, Probability density of orbital angular momentum mode of autofocusing Airy beam carrying power-exponent-phase vortex through weak anisotropic atmosphere turbulence Opt. Express 25(13), 15286 15298 (2017)

[6] Jennifer C. Ricklin and Frederic M. Davidson, Atmospheric turbulence effects on a partially coherent Gaussian beam: implications for free-space laser communication, J. Opt. Soc. Am. A 19, 1794-1802 (2002).

[7] G. Gbur and E. Wolf, Spreading of partially coherent beams in random media, J. Opt. Soc. Am. A 19 (2002).

[8] Olga Korotkova, Larry C. Andrews, Ronald L. Phillips, "Model for a partially coherent Gaussian beam in atmospheric turbulence with application in Lasercom," Opt. Eng. 43 (2004),

[9] O. Korotkova, *Random Light Beams: Theory and Applications* (CRC Press, Boca Raton, 2014).

[10] Greg Gbur, "Partially coherent beam propagation in atmospheric turbulence [Invited]," J. Opt. Soc. Am. A 31, 2038-2045 (2014).

[11] J. M. Martin and Stanley M. Flatté, "Intensity images and statistics from numerical simulation of wave propagation in 3-D random media," Appl. Opt. 27, 2111-2126 (1988).

[12] J.D. Schmidt, *Numerical Simulation of Optical Wave Propagation with Examples in MATLAB* (SPIE, 2010).

[13] R. F. Lutomirski and H. T. Yura, 'Propagation of a Finite Optical Beam in an Inhomogeneous Medium,' Appl. Opt. 10, 1652-1658 (1971).

[14] L. C. Andrews and R. L. Phillips, "Laser Beam Propagation through Random Media" (SPIE, 2005)

[15] G. Gbur and O. Korotkova, 'Angular spectrum representation for the propagation of arbitrary coherent and partially coherent beams through atmospheric turbulence,' J. Opt. Soc. Am. A 24 (2007).

[16] Fei Wang and Olga Korotkova, "Convolution approach for beam propagation in random media," Opt. Lett. 41, 1546-1549 (2016).

[17] Emil Wolf, 'New theory of partial coherence in the space frequency domain. Part I: spectra and cross spectra of steady-state sources,' J. Opt. Soc. Am. 72, 343 351 (1982).

[18] A. Stuart and J. K. Ord, Kendall Advanced Theory of Statistics, 5th ed., Vol. 1 (Oxford University Press, New York, 1987).

[19] S. Lin, C. Wang, X. Zhu, R Lin, F. Wang, G. Gbur, Y. Cai, J Yu, " Propagation of radially polarized Hermite non-uniformly correlated beams in a turbulent atmosphere " Opt. Exp. 28 (2020).

[20] J. Zeng, C. Liang, H. Wang, F. Wang, C. Zhao, G. Gbur, and Y. Cai, 'Partially coherent radially polarized fractional vortex beam,' Opt. Express 28, 11493 11513 (2020).

[21] Stephen M. Wandzura, "Meaning of quadratic structure functions," J. Opt. Soc. Am. 70, 745-747 (1980)

[22] J.C. Leader, "Atmospheric propagation of partially coherent radiation," J. Opt. Soc. Am. 68, 175-185 (1978).

[23] Greg Gbur and Emil Wolf, "Spreading of partially coherent beams in random media," J. Opt. Soc. Am. A 19, 1592-1598 (2002).

[24] L. Mandel and E. Wolf, Optical Coherence and Quantum Optics (Cambridge University, (1995))

[25] Y. Li, Z. Wu, R. Wu and J. Zhang, "Characteristics of the partially coherent Gaussian Schell-model beam propagating in atmospheric turbulence," 2011 IEEE International Conference on Microwave Technology and Computational Electromagnetics, 2011, pp. 338-341, doi: 10.1109/ICMTCE.2011.5915527

CHAPTER 3: CIRCULARLY COHERENT VORTEX BEAMS OPTIMIZED FOR PROPAGATION THROUGH TURBULENCE

3.1 Abstract

Self-focusing partially coherent beams with circular coherence have shown high potential for robust propagation through atmospheric turbulence. In this paper, we introduce a criteria to approximate the degrading effects of turbulence and we show that how the coherence of the source can be optimized to generate a beam with the highest stability in turbulence. To test our prediction, we analytically compare the turbulence propagation of the OAM spectrum of circularly coherent Gaussian vortex sources with three different coherence parameters. It is shown that by satisfying the introduced optimizing conditions, we can minimize the adverse effects of turbulence on the OAM spectrum.

3.2 Introduction

Beams carrying orbital angular momentum (OAM) have recently been the subject of extensive research due to their potential benefits in a wide variety of applications, including microscopy [1], spectroscopy [2] and optical communications [3, 4]. The canonical example of OAM beams is the set of Laguerre-Gauss beams, which possess a singularity of phase on their central axis and an integer helical phase twist – an optical vortex – around that axis; these beams also possess an orbital angular momentum proportional to the phase twist [5]. The Laguerre-Gauss beams can be multiplexed and demultiplexed through a geometric mode sorter [6], potentially allowing for a dramatic increase in amount of data transmitted along a single optical channel in free-space optical communications.

However, it has also been demonstrated that atmospheric turbulence will degrade an OAM signal, causing a pure OAM state to split into a spectrum of modes and resulting in crosstalk and degraded channel capacity in an OAM-based communications system [7, 8]. To circumvent this, beams with non-trivial phase, amplitude, polarization, and coherence have been studied as alternatives, and the study of such beams is now referred to as structured light [9].

One promising possibility of structured light is the use of beams with reduced spatial coherence. It is known that partially coherent beams exhibit resistance to the degrading effects of turbulence in many cases [10], and it is natural to ask if reducing the spatial coherence of OAM beams can reduce the crosstalk they experience. However, there is a natural conflict between partial coherence and OAM: optical vortices are coherent phase structures in a wavefield, and partial coherence involves the randomization of the phase of a wavefield. There has been extensive research on partially coherent vortex beams [11, 12], and it is widely recognized that the OAM spectrum of a partially coherent vortex beam is, in general, broadened over many modes, because the azimuthal phase of the beam is randomized.

One class of partially coherent beams that do not suffer from such limitations are beams with so-called circular coherence, first introduced in 2017 [13]. In such beams, the field is only partially coherent in the radial direction, but fully coherent in the azimuthal direction. Such beams may be considered as an ensemble of beams with random focal distances, which also indicates that these beams tend to have self-focusing properties. Though the original paper on circular coherence considered non-vortex beams, it can readily be shown that a circularly coherent beam with an embedded vortex phase, and associated pure OAM state, will maintain that state on propagation in free space [14]. Such beams, with a pure OAM state and partial coherence along the radial direction, are potentially more resistant to the effects of atmospheric turbulence and a possible means of improving channel robustness in

free-space optical communications.

In this paper, we analytically model the propagation of circularly coherent vortex beams in atmospheric turbulence under various conditions. We provide guidelines for optimizing such beams for a given turbulence channel, and discuss the physics of the results. We show how this type of beam can be produced in a simple way and how we can modulate a beam at its source to increase the stability of its OAM spectrum against turbulence fluctuations.

3.3 Vortex Beams With Circular Coherence

We begin by introducing the notation and theory related to the class of circularly coherent vortex beams. Partially coherent beams in general can be characterized by the cross-spectral density (CSD) function, which is defined as the correlation between the fields at two different points $\boldsymbol{\rho}_1$ and $\boldsymbol{\rho}_2$ in the beam cross-section at frequency ω,

$$W(\boldsymbol{\rho}_1, \boldsymbol{\rho}_2, \omega) = \left\langle U^*(\boldsymbol{\rho}_1, \omega) U(\boldsymbol{\rho}_2, \omega) \right\rangle_\omega \ , \tag{3.1}$$

where $\langle ... \rangle_\omega$ represents the average over an ensemble of monochromatic realizations of the fields [15] and the asterisk represents the complex conjugation. Here $U(\boldsymbol{\rho}, \omega)$ represents the field at vector position $\boldsymbol{\rho}$ in the transverse plane at frequency ω. We note that the spatial coherence properties of a quasi-monochromatic field can be well-characterized by the cross-spectral density at its center frequency ω; we suppress explicit mention of frequency in the arguments of functions going forward for brevity.

In general, it is well-known that the cross-spectral density may always be represented in terms of its coherent field characteristics, characterized by $\tau(\boldsymbol{\rho})$, and its spectral degree of coherence $\mu(\boldsymbol{\rho}_1, \boldsymbol{\rho}_2)$, in the form

$$W(\boldsymbol{\rho}_1, \boldsymbol{\rho}_2) = \tau^*(\boldsymbol{\rho}_1) \tau(\boldsymbol{\rho}_2) \mu(\boldsymbol{\rho}_1, \boldsymbol{\rho}_2), \tag{3.2}$$

where $0 \leq |\mu(\boldsymbol{\rho}_1, \boldsymbol{\rho}_2)| \leq 1$ for any pair of points.

Circular coherence represents the special case in which the spectral degree of coherence between the two points depends only on their radial separation distance in the form $|\rho_1^2 - \rho_2^2|$. The CSD of this type of beam is written as

$$W(\boldsymbol{\rho}_1, \boldsymbol{\rho}_2) = \tau^*(\boldsymbol{\rho}_1)\tau(\boldsymbol{\rho}_2)\mathbf{g}\left(\rho_1^2 - \rho_2^2\right) \quad , \tag{3.3}$$

where the function $\mathbf{g}$ quantifies the coherence properties of the corresponding beam, with $\mathbf{g}(0) = 1$. We can define such a partially coherent source through the superposition integral [16]

$$W(\boldsymbol{\rho}_1, \boldsymbol{\rho}_2) = \int_{-\infty}^{\infty} d\nu\, \mathtt{p}(\nu) H^*(\boldsymbol{\rho}_1, \nu) H(\boldsymbol{\rho}_2, \nu) \quad , \tag{3.4}$$

where $\mathtt{p}(\nu)$ is a non-negative Fourier transformable weight function. By choosing the kernel $H(\boldsymbol{\rho}, \nu)$ as a coherent field with a finite radius of curvature [17]

$$H(\boldsymbol{\rho}, \nu) = \tau(\boldsymbol{\rho}) e^{-2\pi i \nu \rho^2} \quad , \tag{3.5}$$

the resulting CSD can be interpreted as the incoherent superposition of coherent beams with different radii of curvature; this curvature is defined as a function of the distribution variable ν as

$$R_0(\nu) = \frac{1}{2\lambda\nu} \quad , \tag{3.6}$$

where λ is the wavelength. The corresponding CSD can be expressed as

$$W(\boldsymbol{\rho}_1, \boldsymbol{\rho}_2) = \tau^*(\boldsymbol{\rho}_1)\tau(\boldsymbol{\rho}_2)\tilde{\mathtt{p}}(\rho_1^2 - \rho_2^2) \quad , \tag{3.7}$$

where we have used tilde to represent the Fourier transform.

Various distribution functions have Fourier transforms that meet the conditions

of circular coherence, including Gaussian, Lorentzian, and rectangular distributions. Selecting an appropriate distribution function provides a degree of freedom to optimize the coherence state of the source, thereby improving its resilience to turbulence. For our model, we have opted for the rectangular function as

$$\mathtt{p}(\nu) = \mathrm{Rect}\left(\frac{\nu - \nu_0}{\Delta\nu}\right) \quad , \tag{3.8}$$

where $\mathrm{Rect}(\nu)$ indicates the rectangular function with value 1 for $|\nu| \leq 1/2$ and zero otherwise. Here ν_0 and $\Delta\nu$ are the center and width of the rectangular window, respectively, which should be determined to minimize the turbulence effects. The discussion regarding these parameters will be provided in Section 4.

By considering the function $\tau(\boldsymbol{\rho})$ as a 1st order Gaussian vortex beam,

$$\tau(\boldsymbol{\rho}) = \rho e^{i\phi} \exp\left(-\frac{\rho^2}{2\sigma_s^2}\right), \tag{3.9}$$

where ϕ and σ_s represent the azimuthal angle and beam size, respectively, the CSD of the resulting OAM carrying vortex beam with circular coherence takes the following form,

$$\begin{aligned} W_0(\boldsymbol{\rho}_1, \boldsymbol{\rho}_2) = \rho_1\rho_2 e^{i(\phi_2-\phi_1)} \exp\left[-\frac{1}{2\sigma_s^2}(\rho_1^2 + \rho_2^2)\right] \\ \times \int_{-\infty}^{\infty} d\nu\, \mathtt{p}(\nu) \exp\Big[-2\pi i\nu(\rho_2^2 - \rho_1^2)\Big] \ , \end{aligned} \tag{3.10}$$

where it is to be noted that the azimuthal phase terms are separable, indicating full coherence in the azimuthal direction.

3.4 Propagation Through Atmospheric Turbulence

We now turn to the propagation of circularly coherent beams through atmospheric turbulence; the relevant notation is illustrated in Fig. 3.1. The propagation of the CSD of a partially coherent beam from the points $\boldsymbol{\rho}_1$ and $\boldsymbol{\rho}_2$ in the source plane to

the points $\mathbf{r}_1$ and $\mathbf{r}_2$ in the detector plane at distance z through turbulence can be described by the extended Huygens-Fresnel principle [18],

$$\begin{aligned} W_{turb}(\mathbf{r}_1, \mathbf{r}_2; z) = \left(\frac{k}{2\pi z}\right)^2 \iint d^2\rho_1 \iint d^2\rho_2 \, W_0(\boldsymbol{\rho}_1, \boldsymbol{\rho}_2) \\ \times \exp\left[-\frac{ik}{2z}\Big(|\mathbf{r}_1 - \boldsymbol{\rho}_1|^2 - |\mathbf{r}_2 - \boldsymbol{\rho}_2|^2 \Big)\right] \\ \times \Big\langle \exp\left[\Psi^*(\boldsymbol{\rho}_1, \mathbf{r}_1) + \Psi(\boldsymbol{\rho}_2, \mathbf{r}_2)\right] \Big\rangle, \end{aligned} \tag{3.11}$$

where $k = 2\pi/\lambda$ is the wave number and $\Psi(\boldsymbol{\rho}, \mathbf{r})$ represents the complex phase perturbation of the spherical wave originating at $\boldsymbol{\rho}$ and measured at $\mathbf{r}$ due to refractive index fluctuations. The value of this complex phase can be determined up to second order for homogeneous and isotropic turbulence by the method of cumulants [18]. To make the integrals of Eq. (3.11) tractable, a quadratic approximation for the resulting phase is used, which results in the expression [19]

$$\Big\langle \exp\left[\Psi^*(\boldsymbol{\rho}_1, \mathbf{r}_1) + \Psi(\boldsymbol{\rho}_2, \mathbf{r}_2)\right] \Big\rangle = \exp\left[-Q(z)(r^2 + \rho^2 + \boldsymbol{\rho} \cdot \mathbf{r})\right], \tag{3.12}$$

where $\mathbf{r} = \mathbf{r}_2 - \mathbf{r}_1$ and $\boldsymbol{\rho} = \boldsymbol{\rho}_2 - \boldsymbol{\rho}_1$ are the difference vectors at the detector and source planes, respectively and $Q(z)$ is determined by the state of turbulence,

$$Q(z) \equiv \frac{\pi^2 k^2 z}{3} \int_0^\infty d\kappa \left[\, \kappa^3 \, \Phi_n(\kappa) \,\right] \ , \tag{3.13}$$

where κ is the magnitude of the spatial frequency of the refractive index fluctuations and $\Phi_n(\kappa)$ represents the spatial power spectrum of the turbulence. The four-fold integral of Eq. (3.11) is generally difficult to evaluate. We have simplified the process by using a modified version of the eHF principle [20], which determines the field in the detector plane as a two-fold integral of the free-space propagated version of the

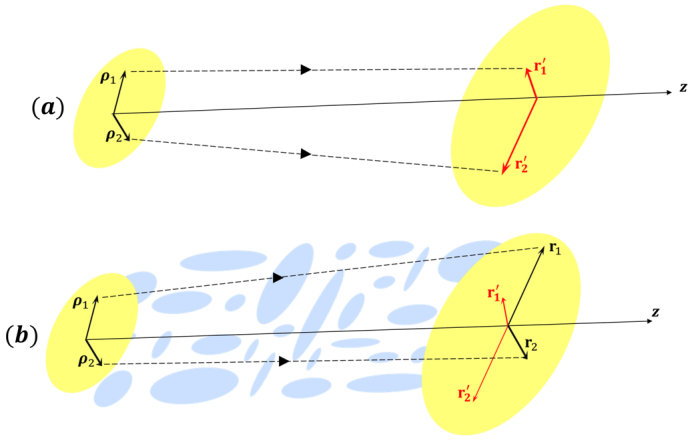

Figure 3.1: (a): Propagation in free space , (b): propagation through turbulence

field. This integral has the form,

$$W_{turb}(\mathbf{R},\mathbf{r};z) = F(\mathbf{R},\mathbf{r};z)\iint d^2R'\,\tilde{W}_{fs}(\mathbf{R}',\mathbf{r}'=\mathbf{r};z) \times \exp\left(-\frac{1}{w^2}R'^2+\frac{2}{w^2}\mathbf{R}'\cdot\mathbf{R}-\frac{3ik}{2z}\mathbf{R}'\cdot\mathbf{r}\right) \quad , \tag{3.14}$$

with

$$F(\mathbf{R},\mathbf{r};z) = \frac{1}{\pi w^2}\exp\left(-\frac{3Q(z)}{4}r^2\right)\exp\left(-\frac{1}{w^2}R^2\right)\exp\left(\frac{3ik}{2z}\mathbf{R}\cdot\mathbf{r}\right), \tag{3.15}$$

$$w^2 = \frac{4z^2Q(z)}{k^2}, \tag{3.16}$$

where $\tilde{W}_{fs}$ represents the CSD of the beam at two points $\mathbf{r}'_1$ and $\mathbf{r}'_2$ in the detector plane in free space propagation as a function of the following sum and difference position vectors,

$$\begin{aligned} \mathbf{r} &= \mathbf{r}_2-\mathbf{r}_1 \quad , \quad \mathbf{R} = \frac{\mathbf{r}_2+\mathbf{r}_1}{2}, \\ \mathbf{r}' &= \mathbf{r}'_2-\mathbf{r}'_1 \quad , \quad \mathbf{R}' = \frac{\mathbf{r}'_2+\mathbf{r}'_1}{2} \quad . \end{aligned} \tag{3.17}$$

Figure 3.1 schematically illustrates the position vectors on the source and detector planes for propagation both in free space and through turbulence.

3.4.1 Free space

To evaluate Eq. (3.14), we first need to evaluate the propagation of the CSD function in free space by applying Fresnel propagation. In this paper the term "free space" means "in the absence of turbulence effects." The most elegant approach is simply to evaluate the integrand of Eq. (3.10) while leaving the integral over ν to be done numerically. In terms of position vectors $\mathbf{r}_1'$ and $\mathbf{r}_2'$, the CSD in the detector plane becomes

$$\begin{aligned}\tilde{W}_{fs}(\mathbf{r}_1', \mathbf{r}_2'; z) = \int_{-\infty}^{\infty} d\nu\, \mathtt{p}'(\nu)\, z_1'^{*} z_2' \exp\left[-\frac{1}{2\sigma_s'^2(\nu)}\left(r_1'^2 + r_2'^2\right)\right] \\ \times \exp\left[-\frac{ik}{2R_z'(\nu)}(r_1'^2 - r_2'^2)\right] \quad ,\end{aligned} \tag{3.18}$$

where we have introduced $z_i' = x_i' + iy_i'$, with $i = 1, 2$. Similar to the expression for the CSD in the source plane, the Eq. (3.18) represents the CSD function in the detector plane as a superposition of beams with different sizes $\sigma_s'(\nu)$ and radii of curvature $R_z'(\nu)$ in free space determined by the probability variable ν and with a new weight function $\mathtt{p}'(\nu)$; these equantities are given by

$$\mathtt{p}'(\nu) = t^4(\nu)\mathtt{p}(\nu), \tag{3.19}$$

$$\sigma_s'^2(\nu) = \sigma_s^2\left[\beta^2(\nu) + \left(\frac{z}{z_0}\right)^2\right], \tag{3.20}$$

$$\frac{1}{R_z'(\nu)} = \frac{1 - t^2(\nu)\beta(\nu)}{z}, \tag{3.21}$$

where $z_0 = k\sigma_s^2$ is the Rayleigh range of a Gaussian beam and the parameters $t(\nu)$ and $\beta(\nu)$ are defined as

$$\beta(\nu) = 1 - \frac{z}{R_0(\nu)}, \tag{3.22}$$

$$t(\nu) = \frac{\sigma_s}{\sigma_s'(\nu)}. \tag{3.23}$$

3.4.2 Turbulence

Substituting from Eq. (3.18) into Eq. (3.14), the CSD in the detector plane after propagation through turbulence can be obtained in terms of position vectors $\mathbf{r}_1$ and $\mathbf{r}_2$ as

$$\begin{aligned} W_{turb}(\mathbf{r}_1,\mathbf{r}_2;z) = \int_{-\infty}^{\infty} \Big\{ C_0(\nu) + C_1^*(\nu) z_1^2 + C_1(\nu) z_2^2 + C_2(\nu) z_1^* z_2 + \big[C_2(\nu) - 1\big] z_1 z_2^* \Big\} \\ \times \exp\left[-\frac{1}{2\Sigma_s^2(\nu)} \left(r_1^2 + r_2^2 \right) \right] \exp\left[-\frac{1}{2\Sigma_g^2(\nu)} |\mathbf{r}_1 - \mathbf{r}_2|^2 \right] \\ \times \exp\left[-\frac{ik}{2R_z(\nu)} (r_1^2 - r_2^2) \right] d\nu\, \mathcal{P}(\nu). \end{aligned} \tag{3.24}$$

This equation shows that the resulting CSD function has the form of a superposition of Schell-model partially coherent vortex beams of orders 0, -1, $+1$ with the weight function $\mathcal{P}(\nu)$ and different beam sizes $\Sigma_s(\nu)$, coherence widths $\Sigma_g(\nu)$ and radii of curvature $R_z(\nu)$, defined as

$$\mathcal{P}(\nu) = T^4(\nu) \mathtt{p}'(\nu), \tag{3.25}$$

$$\Sigma_s^2(\nu) = \sigma_s'^2(\nu) + Q(z) \left(\frac{4z^2}{k^2} \right), \tag{3.26}$$

$$\frac{1}{2\Sigma_g^2(\nu)} = \frac{1}{4\sigma_s'^2(\nu)} - \frac{1}{4\Sigma_s^2(\nu)} + Q(z) \left[\frac{z\, T(\nu)}{\widehat{R}_z(\nu)} \right]^2 + \frac{3}{4} Q(z), \tag{3.27}$$

$$\frac{1}{R_z(\nu)} = \frac{3}{2z} + \frac{T^2(\nu)}{\widehat{R}_z(\nu)}, \tag{3.28}$$

where the parameters $T(\nu)$ and $\widehat{R}_z(\nu)$ are

$$\frac{1}{\widehat{R}_z(\nu)} = \frac{1}{R_z'(\nu)} - \frac{3}{2z} \ , \tag{3.29}$$

$$T(\nu) = \frac{\sigma_s'(\nu)}{\Sigma_s(\nu)} \ . \tag{3.30}$$

The parameters C_i, with $i = 0, 1, 2$ may be interpreted as relative weights of the different vortex terms of Eq. (3.24); these have the form

$$C_0(\nu) = Q(z)\left(\frac{4z^2}{k^2}\right), \tag{3.31}$$

$$C_1(\nu) = \frac{1}{4}\left[T^2(\nu) - \frac{1}{T^2(\nu)}\right] + Q^2(z)\left[\left(\frac{2z^2}{k}\right)\frac{T(\nu)}{\widehat{R}_z(\nu)}\right]^2 + iQ(z)\left[\left(\frac{2z^2}{k}\right)\frac{T^2(\nu)}{\widehat{R}_z(\nu)}\right], \tag{3.32}$$

$$C_2(\nu) = \frac{1}{4}\left[T^2(\nu) + \frac{1}{T^2(\nu)}\right] + Q^2(z)\left[\left(\frac{2z^2}{k}\right)\frac{T(\nu)}{\widehat{R}_z(\nu)}\right]^2 + \frac{1}{2}\,. \tag{3.33}$$

The expression for the CSD on propagation through turbulence given in Eq. (3.24) recovers the free space result of Eq. (3.18) in the limit $Q(z) \to 0$, which results in $T(\nu) = 1$.

3.5 OAM spectrum

With the results of the prevous sections, we can now turn to evaluating the effect of atmospheric turbulence on the OAM spectrum of circularly coherent vortex beams. The OAM spectrum is determined by finding the intensity associated with each azimuthal mode of the field. We may find this by first decomposing the CSD in terms of its azimuthal modes,

$$W_m(r_1, r_2) = \frac{1}{(2\pi)^2}\int_0^{2\pi}\int_0^{2\pi} d\phi_1 d\phi_2 W(\mathbf{r}_1, \mathbf{r}_2) e^{im(\phi_1 - \phi_2)}\ , \tag{3.34}$$

where r_1, r_2 and ϕ_1, ϕ_2 represent the radial and azimuthal coordinates, respectively, corresponding to the position vectors $\mathbf{r}_1$ and $\mathbf{r}_2$. We substitute from Eq. (3.24) into Eq. (3.34) to find this azimuthal modal distribution. We then find the total intensity associated with each mode by setting $r_1 = r_2 \equiv r$ and integrating over the radius of

the detector aperture $\mathtt{R}_d$; the intensity of the mth mode is given by the expression,

$$
\begin{aligned}
I_m = 2\pi \int_0^{\mathtt{R}_d} r dr \int_{-\infty}^{\infty} d\nu\, \mathcal{P}(\nu) \exp\left[-\left(\frac{1}{\Sigma_s^2}+\frac{1}{\Sigma_g^2}\right) r^2\right] \\
\times \left\{ \Big[C_0(\nu) + 2\Re\left\{C_1(\nu)\right\} r^2\Big] \mathcal{I}_m\left(\frac{r^2}{\Sigma_g^2}\right) + C_2(\nu) r^2 \mathcal{I}_{m-1}\left(\frac{r^2}{\Sigma_g^2}\right) \right. \\
\left. + \Big[C_2(\nu) - 1\Big] r^2 \mathcal{I}_{m+1}\left(\frac{r^2}{\Sigma_g^2}\right) \right\},
\end{aligned}
\tag{3.35}
$$

where $\mathcal{I}_m$ is the modified Bessel function of order m. This result can be used to find the OAM spectrum of both coherent and circularly coherence beams in turbulence propagation, with the coherent case given by $R_0(\nu) \to \infty$, which is equivalent to $\nu \to 0$.

We must also integrate over the curvature variable ν, using the form of Eq. (3.8) for $\mathtt{p}(\nu)$. Our goal is to find the values of ν_0 and $\Delta\nu$, the center and width of the rectangular window, respectively, such that the effects of turbulence on the OAM spectrum are minimized.

It is well-known that turbulence degrades the quality of the beam by increasing the beam size and reducing its correlation length. Therefore, we may examine the ratio of the correlation length over beam size as a measure of turbulence resistance, i.e.

$$
\Omega \equiv \frac{\Sigma_g}{\Sigma_s} \quad . \tag{3.36}
$$

By analyzing the profile of Ω for various values of ν, we have found that its maximum happens at $\nu = 3/4\lambda z$, which is equivalent to a radius of curvature of $R_0 = 2z/3$, and this is independent of the beam size at source, the strength of turbulence and the propagation distance.

As an example, Fig. 3.2 shows the profile of Ω for a beam with $\sigma_s = 3$ cm in $z = 600$ m propagation through moderate strength turbulence. As is evident, the maximum of Ω happens at $\nu = 3/4\lambda z$. This suggests that we may create a beam with

strong turbulence resistance by assigning a narrow rectangular window for $\mathtt{p}(\nu)$ with a width of $\Delta\nu$ and the center $\nu_0 = 3/4\lambda z$, as is shown by the red region in Fig. 3.2. Considering the fact that $\nu = 0$ corresponds to the coherent source of a vortex beam with infinite radius of curvature, which has lower value of Ω in Fig. 3.2, we can expect that a circularly coherent beam with the aforementioned parameters is more resistant than its fully coherent counterpart.

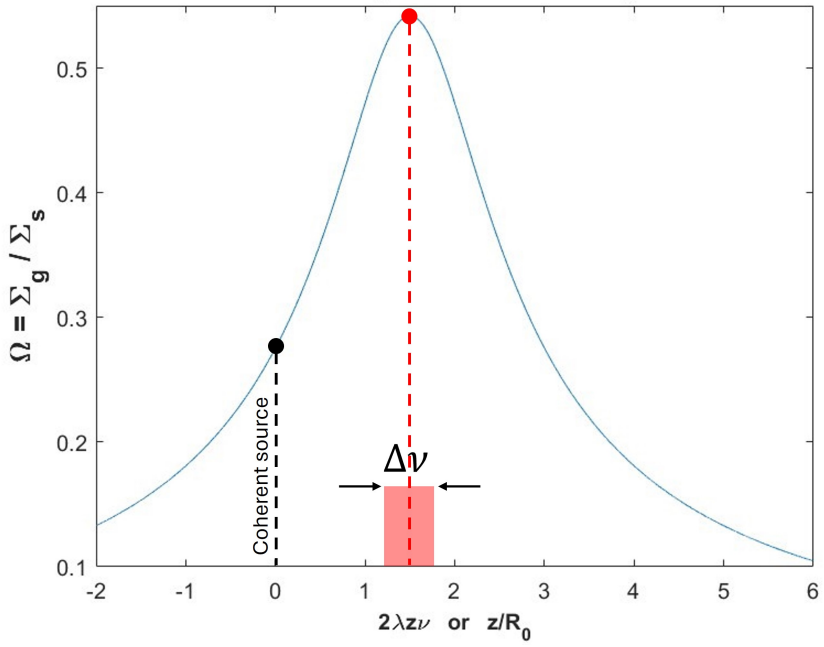

Figure 3.2: Profile of Ω vs. $2\lambda z\nu$ of a circularly coherent beam detected after $z = 600$ m propagation through turbulence with the strength $C_n^2 = 10^{-14}$ m$^{-2/3}$. The beam size at the source is $\sigma_s = 3$ cm.

We approximate the integral over ν in Eq. (3.35) by a discrete finite sum of ν values in the vicinity of ν_0; this is equivalent to superimposing a finite number of Gaussian vortex beams with radii of curvature in the range of $\frac{2z}{3} - \Delta R_0 < R_0 < \frac{2z}{3} + \Delta R_0$ with $\Delta R_0 = \frac{\epsilon}{\lambda\left(\nu_0^2 - \epsilon^2\right)}$,

$$\int_{-\infty}^{\infty} d\nu\, \mathtt{p}(\nu) G(\nu) \;=\; \int_{\nu_0-\epsilon}^{\nu_0+\epsilon} d\nu\, G(\nu) \;\approx\; \sum_{j=1}^{N} G(\nu_j) \qquad , \qquad (\nu_0 - \epsilon < \nu_j < \nu_0 + \epsilon) \tag{3.37}$$

where $\epsilon = \Delta\nu/2$ and $G(\nu)$ represents any arbitrary integrand.

To test our prediction about the relationship between the parameter Ω and the robustness of the featured circularly coherent beam, in Fig. 3.3, we have compared the normalized OAM spectrum of several circularly coherent Gaussian 1st order vortex beams with different values of ν_0 in $z = 500$ m propagation through turbulence.

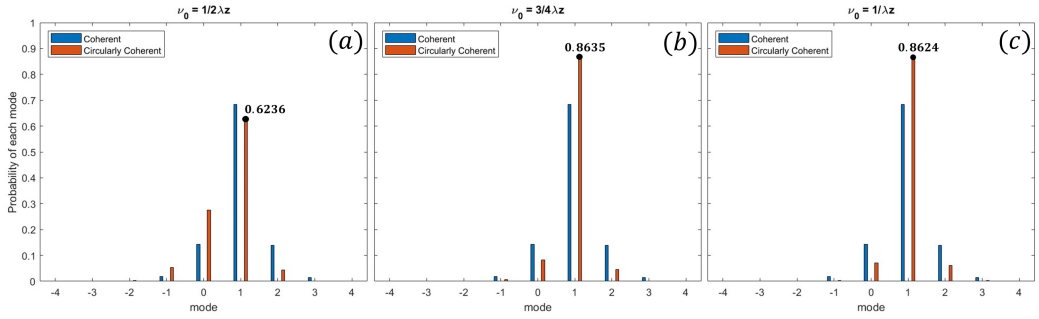

Figure 3.3: Probability distribution of OAM modes detected after $z = 500$ m propagation through turbulence with $C_n^2 = 2 \times 10^{-15}$ m$^{-2/3}$. The beam size at source is $\sigma_s = 2$ cm with wavelength $\lambda = 632$ nm and infinite sized detector $\mathtt{R}_d \to \infty$.

For the power spectrum of turbulence fluctuations we have used the Von-Karman model [18] with the values of 2 mm and 25 m as inner and outer scales, respectively, and a turbulence strength of $C_n^2 = 2 \times 10^{-15}$ m$^{-2/3}$. The number of superimposed beams at source is $N = 6$ and the width of the rectangular distribution is $\Delta\nu = 0.001/\lambda z$ m^{-2}. The blue bars represent the OAM spectrum of a coherent source with $\nu = 0$ and the red bars correspond to a circularly coherent source with $(a) : \nu_0 = 1/2\lambda z$ or $R_0 = z$, $(b) : \nu_0 = 3/4\lambda z$ or $R_0 = 2z/3$, and $(c) : \nu_0 = 1/\lambda z$ or $R_0 = z/2$. Since at the source we had a pure first order vortex beam, a higher concentration of intensity in the first order OAM mode at the detector implies lower disturbance caused by turbulence.

It is evident that the source composed of different beams with radii of curvature close to $R_0 = 2z/3$, or equivalently $\nu_0 = 3/4\lambda z$, shows higher resistance than the other cases, which supports our prediction of Eq. (3.36). Also, we should notice

that the circularly coherent beam with $\nu_0 = 1/2\lambda z$ in Fig. 3.3(a) is impacted by the turbulence more than the coherent beam, which signifies the sensitivity of relationship between the range of radii of curvature of beams at the source and the resistance of the generated beam against turbulence.

Figure 3.4 shows the OAM spectrum for a finite sized detector with radius $\mathtt{R}_d = 5$ cm propagating from a source with the same parameters of Fig. 3.3 through turbulence. A comparison of the two figures shows that the OAM spectrum gets broader when the aperture is finite but still the case with maximum Ω at $\nu_0 = 3/4\lambda z$ has the highest intensity in the mode of order 1, indicating the strongest turbulence resistance.

It should be noted that due to the self-focusing feature of circularly coherent beams, according to the expressions of beam sizes in turbulence given in Eq. (3.20) and Eq. (3.26), the minimum spot size on the detector will be achieved for sources with $\nu_0 = 1/2\lambda z$, which does not provide the most stable OAM spectrum.

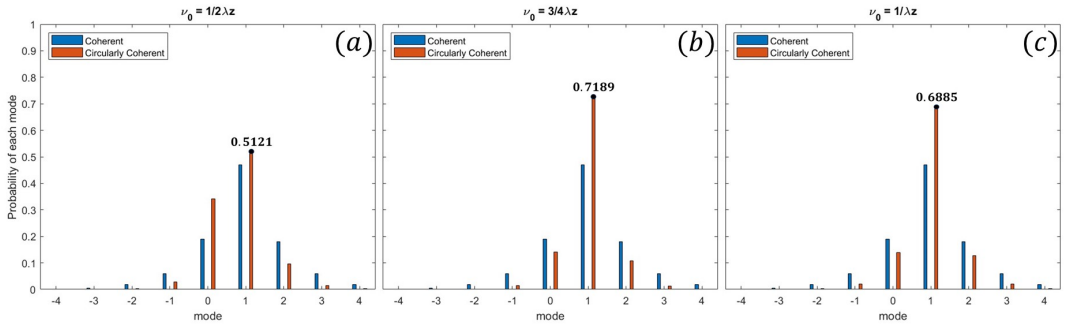

Figure 3.4: Probability distribution of OAM modes detected after $z = 500$ m propagation through turbulence. The beam size at source is $\sigma_s = 2$ cm with wavelength $\lambda = 632$ nm. Radius of the detector is $\mathtt{R}_d = 5$ cm.

We have yet to determine how the width $\Delta\nu$, which is inversely related to the correlation length of the beam, affects the OAM spectrum. Here we must also consider how the number of beams used in the discrete sum of Eq. (3.37) affects our results. In Fig. 3.5, we have plotted the standard deviation of the OAM spectrum in turbulence

for sources with different numbers of beams N and different ranges of $\Delta\nu$. The standard deviation is considered as a rough measure of concentration of energy in the central mode of the spectrum; this implies that a lower standard deviation corresponds to a higher resistance in turbulence. In Fig. 3.5, The solid black dot at $N = 1$ shows the standard deviation corresponding to the coherent source with a single beam with the radius of curvature of $R_0 = 2/3z$.

We may make two observations related to this figure. First, we can see that increasing the range of $\Delta\nu$ reduces the standard deviation of the OAM spectrum. Therefore, the circularly coherent beams do in fact show some improved resistance to turbulence, but it is a relatively small improvement compared to an optimally focused coherent beam. For this class of beams, choosing the optimal focusing is more significant than choosing the optimal coherence.

Second, we note that a relatively small number of beamlets are needed in order to achieve the best turbulence resistance possible for any value of $\Delta\nu$, considering we are using a finite sum to approximate a continuous integral over ν. This appears to be an example of what has been referred to as "beamlet diversity," first observed for Bessel-correlated beams in turbulence [21]. This diversity can be explained as follows. Our partially coherent beam has improved resistance to turbulence by sending mutually incoherent beamlets with different ν parameters through the same realization of turbulence. Each beamlet will propagate through the same turbulence realization and produce a different interference pattern at the detector; if these patterns are very different from each other, we expect that the effects of turbulence will be averaged out. However, beamlets with nearly identical values of ν will produce nearly identical interference patterns and will produce a result no different from a fully coherent beam. In order for beamlets to provide some mutual improvement, they must have sufficiently diverse – very different – values of ν. For a fixed value of $\Delta\nu$, evidently there is an optimum separation of beamlets in ν beyond which they become redundant

and produce no positive effects.

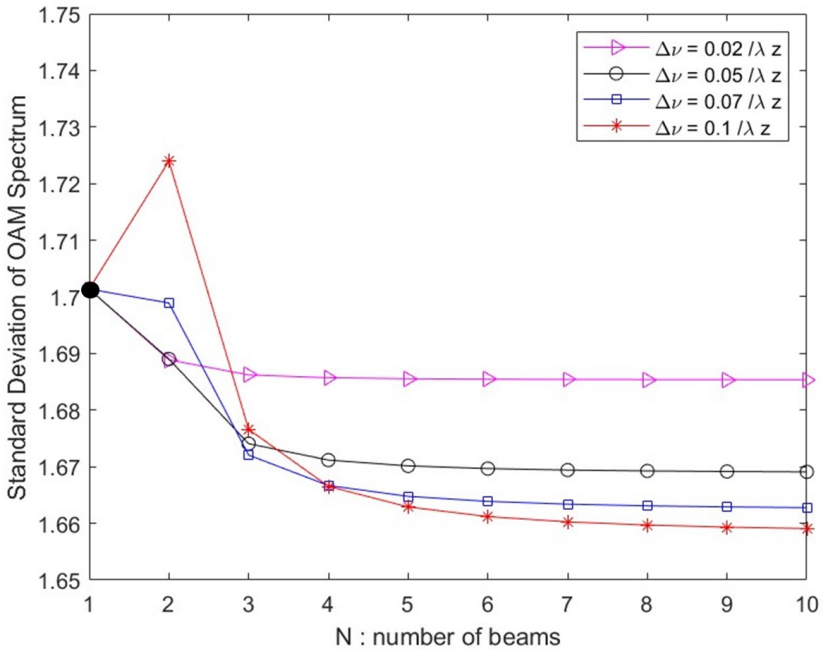

Figure 3.5: Standard deviation of normalized OAM spectrum in turbulence Vs. number of superimposed beams at source (N) for different ranges of radii of curvature around $R_0 = 2/3z$ or equivalently $\nu_0 = 3/4\lambda z$. The beam size at the source is $\sigma_s = 2$ cm and wavelength $\lambda = 632$ nm . The beam is propagated $z = 1$ km through turbulence with the strength of $C_n^2 = 2 \times 10^{-15}$ m$^{-2/3}$.

3.6 Conclusion

In this paper, we have studied the propagation characteristics of circularly coherent vortex beams in atmospheric turbulence for a variety of spatial correlation parameters. We have found that circularly coherent vortex beams, which possess a pure OAM state at the source and on propagation through free space, can show improved resistance in turbulence over their coherent counterparts. This resistance is characterized by the standard deviation of the mode spectrum.

In our calculations, we have determined a parameter Ω that provides an excellent estimate of the optimal choice of partially coherent beam for turbulence resistance. For circularly coherent vortex beams, this parameter depends more on the average wavefront curvature of the constituent beamlets and less on the actual spatial cor-

relation of the beam. We have seen that wavefront curvature plays a greater role in turbulence resistance for this beam class than spatial coherence.

The results highlight a turbulence propagation phenomenon we have referred to as beamlet diversity, in which the constituent beamlets of a partially coherent beam must be sufficiently different from each other in order to strengthen the beam resistance. For circularly coherent vortex beams, relatively few beamlets can be used to approximate a full integral over the beam curvature parameter ν. This is both an advantage, in that it shows that circularly coherent vortex beams can be very easily approximated by a finite set of incoherent beams, and a disadvantage, in that there is evidently not enough beamlet diversity to allow for greater turbulence resistance.

There are, however, more classes of beams that possess a pure azimuthal phase structure and may be considered "circularly coherent vortex beams," including a straightforward incoherent superposition of Laguerre-Gauss beams with the same azimuthal order [22]. Our results provide insight and guidance in how further turbulence resistance can be achieved for partially coherent vortex beams of more general types.

REFERENCES

[1] Ritsch-Marte M. Orbital angular momentum light in microscopy. Philos Trans A Math Phys Eng Sci. 2017 Feb 28;375(2087):20150437. doi: 10.1098/rsta.2015.0437. PMID: 28069768; PMCID: PMC5247481

[2] Fu, S., Zhai, Y., Zhang, J. et al. Universal orbital angular momentum spectrum analyzer for beams. PhotoniX 1, 19 (2020). https://doi.org/10.1186/s43074-020-00019-5

[3] Graham Gibson, Johannes Courtial, Miles J. Padgett, Mikhail Vasnetsov, Valeriy Pasko, Stephen M. Barnett, and Sonja Franke Arnold, "Free space information transfer using light beams carrying orbital angular momentum," Opt. Express 12, 5448 5456 (2004)

[4] A. E. Willner, H. Huang, Y. Yan, Y. Ren, N. Ahmed, G. Xie, C. Bao, L. Li, Y. Cao, Z. Zhao, J. Wang, M. P. J. Lavery, M. Tur, S. Ramachandran, A. F. Molisch, N. Ashrafi, and S. Ashrafi, "Optical communications using orbital angular momentum beams," Adv. Opt. Photon. 7, 66-106 (2015)

[5] L. Allen, M. W. Beijersbergen, R. J. C. Spreeuw, and J. P. Woerdman, "Orbital angular momentum of light and the transformation of Laguerre-Gaussian laser modes," Phys. Rev. A 45, 8185 (1992).

[6] M. Mirhosseini, M. Malik, Z. Shi, and R.W. Boyd, "Efficient separation of the orbital angular momentum eigenstates of light," Nat Commun 4, 2781 (2013).

[7] M. Malik, M. O Sullivan, B. Rodenburg, M. Mirhosseini, J. Leach, M.P.J. Lavery, M.J. Padgett, and R.W. Boyd, "Influence of atmospheric turbulence on optical communications using orbital angular momentum for encoding," Opt. Express 20, 13195-13200 (2012).

[8] B. Rodenburg, M.P.J. Lavery, M. Malik, M.N. O Sullivan, M. Mirhosseini, D.J. Robertson, M. Padgett, and R.W. Boyd, "Influence of atmospheric turbulence on states of light carrying orbital angular momentum," Opt. Lett. 37, 3735-3737 (2012).

[9] O.V. Angelsky, A.Y. Bekshaev, S.G. Hanson, C.Y. Zenkova, I.I. Mokhun, and J. Zheng, "Structured Light: Ideas and Concepts," Front. Phys. 8:114 (2020).

[10] Greg Gbur, "Partially coherent beam propagation in atmospheric turbulence [Invited]," J. Opt. Soc. Am. A 31, 2038-2045 (2014).

[11] J. Zeng, K. Lin, X. Liu, C. Zhao and Y. Cai, 'Review on partially coherent vortex beams,' Front. Optoelectron. 12, 229 248 (2019).

[12] M. Dong, C. Zhao, Y. Cai, and Y. Yang, Partially coherent vortex beams: Fundamentals and applications," Sci. China Phys. Mech. Astron. 64, 224201 (2021).

[13] M. Santarsiero, R. MartÃnez-Herrero, D. Maluenda, J. C. G. de Sande, G. Piquero, and F. Gori, "Partially coherent sources with circular coherence," Opt. Lett. 42, 1512-1515 (2017).

[14] R. Qi, A. Shiri and G. Gbur, "Circularly coherent vortex beams," in preparation.

[15] E. Wolf, 'New theory of partial coherence in the space frequency domain. Part I: spectra and cross spectra of steady state sources,' J. Opt. Soc. Am. 72, 343 351 (1982).

[16] F. Gori and M. Santarsiero, "Devising genuine spatial correlation functions," Opt. Lett. 32, 3531-3533 (2007).

[17] Chaoliang Ding, Matias Koivurova, Jari Turunen, and Liuzhan Pan, "Self-focusing of a partially coherent beam with circular coherence," J. Opt. Soc. Am. A 34, 1441-1447 (2017).

[18] L. C. Andrews and R. L. Phillips, "Laser Beam Propagation through Random Media" (SPIE, 2005)

[19] S. Lin, C. Wang, X. Zhu, R. Lin, F. Wang, G. Gbur, Y. Cai, and J. Yu, 'Propagation of radially polarized Hermite non-uniformly correlated beams in a turbulent atmosphere,' Opt. Express 28, 27238 27249 (2020)

[20] Arash Shiri, Jason Schmidt, Jason Tellez, and Greg Gbur, "Modified Huygens Fresnel method for the propagation of partially coherent beams through turbulence," J. Opt. Soc. Am. A 40, 470 478 (2023).

[21] Yalong Gu and Greg Gbur, "Scintillation of pseudo-Bessel correlated beams in atmospheric turbulence," J. Opt. Soc. Am. A 27, 2621-2629 (2010).

[22] Galina V. Bogatyryova, Christina V. Fel de, Peter V. Polyanskii, Sergey A. Ponomarenko, Marat S. Soskin, and Emil Wolf, 'Partially coherent vortex beams with a separable phase,' Opt. Lett. 28, 878 880 (2003).

CHAPTER 4: ORBITAL ANGULAR MOMENTUM SPECTRUM OF MODEL PARTIALLY COHERENT BEAMS IN TURBULENCE

ABSTRACT

ARASH SHIRI. Orbital Angular Momentum of Partially Coherent Beams Through Atmospheric Turbulence. (Under the direction of DR. GREG GBUR)

The use of partial coherence has been extensively studied as a potential solution to mitigate the destructive effects of atmospheric turbulence in optical applications involving the free space propagation of light. However, in OAM-based optical systems, reducing coherence leads to the broadening of the orbital angular momentum (OAM) spectrum, consequently increasing the cross-talk between adjacent modes. In this paper, we have investigated three fundamental classes of partially coherent OAM beams under the influence of turbulence. The aim is to identify a distinct type of partially coherent beam (PCB) in which the reduction in coherence results in higher resistance of the OAM spectrum against atmospheric disturbances. It is demonstrated that, for a specific propagation distance, we can prepare a PCB in which the benefits of reducing coherence outweigh its drawbacks.

4.1 Introduction

In the realm of optical communication, the quest for higher data transfer rates has led researchers to explore innovative solutions beyond conventional techniques which primarily rely on intensity, wavelength, and polarization modulation for data encoding [1]. A promising solution involves utilizing the orbital angular momentum (OAM) of light. OAM, arising from the helical phase front of the light beam, provides an extra degree of freedom, in addition to the traditional schemes. This property enables the encoding of multiple information channels onto a single beam of light via different OAM values. As a result, OAM-based communication systems have the potential to achieve unprecedented data rates, making them particularly useful for applications requiring high capacity data channels [2].

However, over significant propagation distances in free space, atmospheric turbulence induces fluctuations in the field, thereby degrading the quality of the optical beams. Specifically, turbulence effects on OAM-carrying beams result in a broadening of the OAM spectrum, consequently limiting the capacity of channels due to increased cross-talk. Addressing this challenge necessitates a comprehensive fundamental study of the effects of the fluctuations of refractive index on the light beam, particularly its OAM spectrum. However, owing to the complex nature of turbulence, researchers have encountered considerable difficulties in optimizing the interaction of light with random media. To circumvent this challenge, structured light fields with non-trivial phase, amplitude, polarization, and coherence have been investigated as a means to improve propagation characteristics.

It has been demonstrated that partially coherent beams (PCBs) exhibit higher resistance against turbulence fluctuations [3, 4, 5]. This suggests that we can mitigate the degrading effects of turbulence on the OAM spectrum by reducing the spatial coherence of beams. Transitioning from fully coherent to partially coherent can be accomplished by randomizing a characteristic feature of the light field. However, this

randomization typically also affects the phase of light, leading to the redistribution of power in the OAM spectrum, which results in cross-talk between adjacent modes. Therefore, reduction of coherence has advantages and disadvantages for the reliability of data channels in propagation through turbulence. Detailed investigations are required to determine if the advantages can be leveraged to overcome the disadvantages.

Several years ago, Gbur noted that partially coherent OAM beams can be broken into three fundamental classes [6] based on how the OAM is distributed within their cross section. These classes are: (a) PCBs produced by randomizing the position of the beam axis, resulting in a Rankine vortex [7, 8]; such beams are now known as Rankine model beams [9]. (b) PCBs generated by introducing a twist phase into the spatial coherence of the beam, known as twisted Gaussian-Schell model beams [10]. (c) PCBs generated with a separable vortex phase, making them fully coherent in the azimuthal direction [11]. We consider a special class of such beams that are now referred to as circularly coherent beams [12, 13]. A circularly coherent vortex beam can be created via an ensemble of coherent vortex beams with varying focal distances, resulting in a field that is partially coherent only in the radial direction.

In this paper, we conduct an analytic study of the turbulence propagation of OAM-carrying beams within the aforementioned three classes of partially coherent vortex beams. We analyze the behavior of the OAM spectrum under the influence of turbulence, and consider the turbulence resistance of each class. The results provide guidelines for selecting the appropriate type of PCB to enhance the reliability of data transmission in optical communication systems, and indicate directions for future research.

4.2 Partial Coherence and Orbital Angular Momentum

We begin by reviewing the relevant theory relating to partially coherent beams and the corresponding OAM spectra of such beams.

Early coherence theory focused on space-time correlation functions that characterized both the spatial and temporal coherence simultaneously. However, researchers in recent years have focused more on the spatial coherence properties of light. In this case, it is natural to use the cross-spectral density (CSD) function $W(\boldsymbol{\rho}_1, \boldsymbol{\rho}_2, \omega)$ that characterizes the spatial correlation between two points at the frequency ω; it can be written as an average over an ensemble of monochromatic fields [14],

$$W(\boldsymbol{\rho}_1, \boldsymbol{\rho}_2, \omega) = \langle U^*(\boldsymbol{\rho}_1, \omega) U(\boldsymbol{\rho}_2, \omega) \rangle_\omega, \tag{4.1}$$

where $\langle \cdots \rangle_\omega$ represents the average over the monochromatic ensemble, $U(\boldsymbol{\rho}, \omega)$ represents the field of a member of the ensemble, and the asterisk denotes complex conjugation. Many optical fields used in applications may be considered quasi-monochromatic, and the cross-spectral density at the central frequency ω then accurately characterizes the overall field; going forward, we will suppress expression of ω as an argument.

The cross-spectral density can be decomposed in a basis of azimuthal modes, often called the spiral spectrum, of the form [15]

$$W(\boldsymbol{\rho}_1, \boldsymbol{\rho}_2) = \sum_l \sum_m W_{lm}(\rho_1, \rho_2) e^{-il\phi_1} e^{im\phi_2}, \tag{4.2}$$

where the functions $W_{lm}(\rho_1, \rho_2)$ can be derived according to the integral,

$$W_{lm}(\rho_1, \rho_2) = \frac{1}{(2\pi)^2} \int_0^{2\pi} \int_0^{2\pi} W(\boldsymbol{\rho}_1, \boldsymbol{\rho}_2) e^{il\phi_1} e^{-im\phi_2} \, d\phi_1 d\phi_2. \tag{4.3}$$

Here, ρ_1, ρ_2 are radial coordinates and ϕ_1 and ϕ_2 are azimuthal coordinates. The quantity $W_{lm}(\rho_1, \rho_2)$ characterizes the spatial correlations between different azimuthal modes of order l and m. Because a pure spiral mode of the form $\exp[il\phi]$ is also a pure OAM state [16], we may also consider the spiral spectrum as a decomposition

of the beam into different OAM modes.

If we consider just a single term of Eq. (4.2) with $l = m$ and let $\boldsymbol{\rho}_1 = \boldsymbol{\rho}_2 = \boldsymbol{\rho}$, we get the transverse intensity of the OAM mode of order m, denoted by $I_m(\rho)$. By integrating this quantity over the detector aperture, we can determine the total measured intensity of the mth mode of orbital angular momentum,

$$I_m = \int_0^{R_d} \rho \, d\rho \, I_m(\rho), \tag{4.4}$$

where R_d is the radius of the detector. It is to be noted that there are now well-established methods to experimentally sort and detect these OAM mode intensities; see, for example, [17].

For more details about OAM spectra in partially coherent fields, see Korotkova and Gbur [18]. In the next section, the extended Huygens-Fresnel principle is introduced as our method of propagating the CSD function through turbulence. Following this, we consider the three fundamental classes of partially coherent vortex beams and the effect of atmospheric turbulence on their mode spectra.

4.3 Propagation Through Turbulence

The propagation of PCBs through atmospheric turbulence is often calculated using the venerable extended Huygens-Fresnel principle (eHF) [19], which can be applied to coherent or partially coherent fields. If we use $\boldsymbol{\rho}_1$ and $\boldsymbol{\rho}_2$ to label the positions at the source and $\mathbf{r}_1$ and $\mathbf{r}_2$ to label the positions at a detector plane a distance L from the source, the extended Huygens-Fresnel principle is of the form,

$$\begin{aligned} W(\mathbf{r}_1, \mathbf{r}_2; L) = &\left(\frac{k}{2\pi L}\right)^2 \iint d^2\rho_1 \iint d^2\rho_2 \, W_0(\boldsymbol{\rho}_1, \boldsymbol{\rho}_2) \\ &\times \exp\left[-\frac{ik}{2L}\left(\, |\mathbf{r}_1 - \boldsymbol{\rho}_1|^2 - |\mathbf{r}_2 - \boldsymbol{\rho}_2|^2 \,\right)\right] \\ &\times \left\langle \, \exp\left[\Psi^*(\boldsymbol{\rho}_1, \mathbf{r}_1) + \Psi(\boldsymbol{\rho}_2, \mathbf{r}_2)\right] \right\rangle_t, \end{aligned} \tag{4.5}$$

where $k = 2\pi/\lambda$ is the free-space wavenumber, λ being the wavelength, $W_0(\boldsymbol{\rho}_1, \boldsymbol{\rho}_2)$ is the cross-spectral density in the source plane, and $\Psi(\boldsymbol{\rho}_1, \mathbf{r}_1)$ represents the complex phase perturbation of the spherical wave originating at $\boldsymbol{\rho}_1$ and measured at $\mathbf{r}_1$ due to the refractive index fluctuations of the atmosphere. The angle brackets $\langle \cdots \rangle_t$ around the complex phase terms represent an ensemble average over the atmospheric turbulence, and this average can be evaluated using the method of cumulants; see for example, Gbur [20]. It should be noted that the ensemble average over the source and over the turbulence are independent.

The general form of the resulting phase perturbation is quite complicated and typically can only be evaluated numerically; in order to make the calculations tractable, a quadratic approximation is employed, leading to the expression [21]

$$\langle \exp\left[\Psi^*(\boldsymbol{\rho}_1, \mathbf{r}_1) + \Psi(\boldsymbol{\rho}_2, \mathbf{r}_2)\right] \rangle_t = \exp\left[-Q(L)(r^2 + \rho^2 + \boldsymbol{\rho} \cdot \mathbf{r})\right], \tag{4.6}$$

where $\mathbf{r} = \mathbf{r}_2 - \mathbf{r}_1$ and $\boldsymbol{\rho} = \boldsymbol{\rho}_2 - \boldsymbol{\rho}_1$ are the difference vectors at the detector and source planes, respectively, and the quantity $Q(L)$ is associated with the characteristic features of turbulence and is defined as

$$Q(L) \equiv \frac{\pi^2 k^2 L}{3} \int_0^\infty [\, \kappa^3 \, \Phi_n(\kappa) \,] \, d\kappa, \tag{4.7}$$

where κ is the magnitude of the spatial frequency of the refractive index fluctuations and $\Phi_n(\kappa)$ represents the spatial power spectrum of the turbulence. Throughout this paper, the Von Karman model is used to specify the power spectrum of refractive index fluctuations, given by [22]

$$\begin{gathered} \Phi_n(\kappa) = 0.033 C_n^2 \frac{\exp\left(-\kappa^2/\kappa_m^2\right)}{(\kappa^2 + \kappa_0^2)^{11/6}}, \quad 0 \le \kappa < \infty. \\ \kappa_m = \frac{5.92}{l_0}, \quad \kappa_0 = \frac{2\pi}{\mathcal{L}_0}. \end{gathered} \tag{4.8}$$

The parameter C_n^2 is a measure of turbulence strength and is in the range of 10^{-17} $\mathrm{m}^{-2/3}$ to 10^{-13} $\mathrm{m}^{-2/3}$ from the weaker to stronger strengths. We will consider the inner scale l_0 as 2 mm and the outer scale $\mathcal{L}_0$ as 15 m throughout.

We now turn to the three fundamental classes of partially coherent vortex beams described earlier to explore the effect of the atmosphere on the OAM spectrum of each class. In this study, we restrict ourselves to beams with OAM equivalent to a vortex of order 1. To simplify our calculations, we employed a modified version of the extended Huygens-Fresnel principle that was recently introduced [23]; this version is mathematically equivalent to the standard eHF, but can be evaluated with only two integrations.

4.4 Rankine model vortex beams

One direct approach for generating partially coherent beams is to create an ensemble of beams with one or more randomly varying parameters; this approach was systematized by Gori and Santarsiero [24]. In constructing partially coherent vortex beams, it is natural to look at ensembles for which every member is a deterministic vortex beam with the same vortex order. The earliest example of such a beam [25] uses the central position $\boldsymbol{\rho}_0$ of the beam as the random variable, with a probability density $P(\boldsymbol{\rho}_0)$; such beams were initially called "beam wander model" beams. The CSD of such beams may be written in the form

$$W_0(\boldsymbol{\rho}_1, \boldsymbol{\rho}_2) = \int_{-\infty}^{\infty} U^*(\boldsymbol{\rho}_1 - \boldsymbol{\rho}_0) U(\boldsymbol{\rho}_2 - \boldsymbol{\rho}_0) P(\boldsymbol{\rho}_0) d^2\rho_0, \tag{4.9}$$

where $U(\boldsymbol{\rho})$ represents a coherent vortex beam. Figure 1(a) illustrates the deviation of the beam axis of a single ensemble member from the central axis by vector $\boldsymbol{\rho}_0$. The beam wander beam, comprising a combination of many ensemble members with varying axes, is depicted in Fig. 1(b).

These beams are now referred to as Rankine vortex beams, as it has been demon-

strated that their normalized OAM flux density takes on the form of a Rankine vortex [8].

4.4.1 Rankine vortex beams at source

Let us construct our Rankine vortex beam from an ensemble of 1st order vortex Gaussian beams in the source plane of the form,

$$U(\boldsymbol{\rho}) = \rho e^{i\phi} \exp\left(-\frac{\rho^2}{w_0^2}\right), \tag{4.10}$$

where ρ and ϕ are the radial and azimuthal coordinates, respectively, and w_0 is the size of the initial coherent beam.

The probability density $P(\boldsymbol{\rho}_0)$ of the beam axis position is taken to be a Gaussian distribution,

$$P(\boldsymbol{\rho}_0) = \frac{1}{\pi\delta^2} \exp\left(-\frac{\rho_0^2}{\delta^2}\right). \tag{4.11}$$

The parameter δ, representing the RMS width of the Gaussian distribution of beam axis positions, may be understood as an inverse measure of spatial coherence. Specifically, $\delta = 0$ signifies a fully coherent case where the beam axis does not wander; with an increase in δ, the coherence decreases. By substituting from Eqs. (4.10) and (4.11) into Eq. (4.9) and evaluating the integral over $\boldsymbol{\rho}_0$, the CSD of the Rankine vortex beam in the source plane may be written as

$$\begin{aligned} W_0(\boldsymbol{\rho}_1, \boldsymbol{\rho}_2) = \left(\frac{\beta_0^4}{\delta^4}\right) \left[\delta^2 + S_1(\rho_1^2 + \rho_2^2) + S_2 z_1^* z_2 + (S_2 - 1)\, z_1 z_2^*\right] \\ \times \exp\left(-\frac{\rho_1^2 + \rho_2^2}{2\sigma_s^2}\right) \exp\left(-\frac{|\boldsymbol{\rho}_1 - \boldsymbol{\rho}_2|^2}{2\sigma_g^2}\right), \end{aligned} \tag{4.12}$$

where we have defined $z_1 \equiv x_1 + iy_1$, and similarly for z_2. The quantities σ_s and σ_g represent the beam size and coherence width, respectively, of the partially coherent

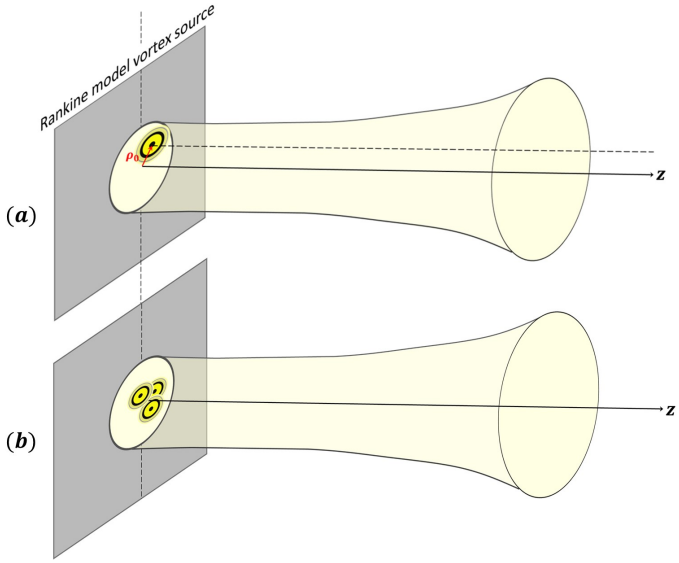

Figure 4.1: The Rankine model source. (a) Deviation from the central axis denoted by $\boldsymbol{\rho}_0$, (b) Combination of multiple beams with varying beam axes.

Rankine model beam, and have the forms

$$\sigma_s^2 = \frac{1}{2}w_0^2 + \delta^2, \tag{4.13}$$

$$\frac{1}{2\sigma_g^2} = \frac{\beta_0^2}{w_0^4}, \tag{4.14}$$

where β_0 and the weight factors S_1, S_2 are defined as

$$\frac{1}{\beta_0^2} \equiv \frac{2}{w_0^2} + \frac{1}{\delta^2}, \tag{4.15}$$

$$S_1 = \delta^2 \left(\frac{1}{2\sigma_g^2} - \frac{1}{w_0^2} \right) \tag{4.16}$$

$$S_2 = \frac{\delta^2}{2\sigma_g^2} + 1. \tag{4.17}$$

As a quadratic formula in terms of the variable $\boldsymbol{\rho}_2$, there will in general be two vortex solutions for a fixed value of $\boldsymbol{\rho}_1$. This already suggests that the OAM spectrum of such a partially coherent beam will be significantly distorted from the coherent case.

4.4.2 Rankine vortex beams in free space

In this paper the term "free space" means "in the absence of turbulence effects." The propagation of the CSD function in free space may be derived from the traditional Huygens-Fresnel diffraction formula,

$$W_{\text{FS}}(\mathbf{r}_1', \mathbf{r}_2'; L) = \left(\frac{k}{2\pi L}\right)^2 \iint d^2\rho_1 \iint d^2\rho_2 W_0(\boldsymbol{\rho}_1, \boldsymbol{\rho}_2) \times \exp\left[-\frac{ik}{2L}\left(|\mathbf{r}_1' - \boldsymbol{\rho}_1|^2 - |\mathbf{r}_2' - \boldsymbol{\rho}_2|^2\right)\right], \tag{4.18}$$

where $\mathbf{r}_1'$ and $\mathbf{r}_2'$ are the position vectors on the detector plane located at distance z. By substituting from Eq. (4.12) into Eq. (4.18), the integrals can be evaluated in the form

$$W_{\text{FS}}(\mathbf{r}_1', \mathbf{r}_2'; L) = \left(\frac{\beta_L^4}{\delta^4}\right)\left(\frac{w_0^4}{w_L^4}\right)\left[\delta^2 + F_1^* r_1'^2 + F_1 r_2'^2 + F_2 z_1'^* z_2' + (F_2 - 1)\, z_1' z_2'^*\right] \times \exp\left(-\frac{r_1'^2 + r_2'^2}{2\sigma_s'^2}\right)\exp\left(-\frac{|\mathbf{r}_1' - \mathbf{r}_2'|^2}{2\sigma_g'^2}\right)\exp\left[-\frac{ik}{2R_L'}(r_1'^2 - r_2'^2)\right]. \tag{4.19}$$

In the above expression, the quantities w_L and σ_s' refer to the beam sizes associated with the initial coherent beam and the partially coherent Rankine model beam during free space propagation to distance L, respectively. Additionally, σ_g' and R_L' represent the coherence width and the average radius of curvature of the Rankine model beam, respectively, after propagation to distance L in free space. These quantities are derived as

$$w_L^2 = w_0^2\left(1 + \frac{L^2}{L_0^2}\right), \tag{4.20}$$

$$\sigma_s'^2 = \frac{1}{2}w_L^2 + \delta^2, \tag{4.21}$$

$$\frac{1}{2\sigma_g'^2} = \frac{\beta_L^2}{w_0^2 w_L^2}, \tag{4.22}$$

$$R_L' = L\left[1 + \frac{L_0^2}{L^2}\left(\frac{\delta^2}{\beta_0^2}\right)\right]. \tag{4.23}$$

In the above expressions, $L_0 = kw_0^2/2$ is the Rayleigh range of the coherent beam. The parameter β_L and the weight factors F_1 and F_2 are introduced as

$$\frac{1}{\beta_L^2} \equiv \frac{2}{w_L^2} + \frac{1}{\delta^2}, \tag{4.24}$$

$$F_1 = -\delta^2 \left(\frac{1}{2\sigma_s'^2} + \frac{1}{2\sigma_g'^2} - \frac{ik}{2R_L'} \right). \tag{4.25}$$

$$F_2 = \frac{\delta^2}{2\sigma_g'^2} + 1. \tag{4.26}$$

It is to be noted that the beam has retained its overall mathematical structure on free-space propagation, as can be seen by comparing Eqs. (4.12) and (4.19).

4.4.3 Rankine vortex beams in turbulence

The propagation of the Rankine vortex beam in turbulence can be found by evaluating Eq. (4.5) for the source given in Eq. (4.12); after some effort, the CSD function through turbulence takes the form

$$\begin{aligned} W_{\text{T}}(\mathbf{r}_1, \mathbf{r}_2; L) = \left(\frac{\beta_L^4}{\delta^4} \right) \left(\frac{w_0^4}{w_L^4} \right) \alpha^4 \left[T_0 + T_1^* r_1^2 + T_1 r_2^2 + T_2 z_1^* z_2 + (T_2 - 1) z_1 z_2^* \right] \\ \times \exp\left(-\frac{r_1^2 + r_2^2}{2\Sigma_s^2} \right) \exp\left(-\frac{|\mathbf{r}_1 - \mathbf{r}_2|^2}{2\Sigma_g^2} \right) \exp\left[-\frac{ik}{2R_L} (r_1^2 - r_2^2) \right], \end{aligned} \tag{4.27}$$

where $\mathbf{r}_1$ and $\mathbf{r}_2$ are the position vectors on the detector plane. The parameters Σ_s, Σ_g and R_z represent the beam size, coherence width and radius of curvature of the beam propagated to the distance L through turbulence, respectively

$$\Sigma_s^2 = \sigma_s'^2 + \left(\frac{4L^2}{k^2} \right) Q(L), \tag{4.28}$$

$$\frac{1}{2\Sigma_g^2} = \frac{1}{2\sigma_g'^2} + \frac{1}{4\sigma_s'^2} - \frac{1}{4\Sigma_s^2} + \left(\frac{3}{4} + \frac{\alpha^2 L^2}{\widehat{R}_L^2} \right) Q(L), \tag{4.29}$$

$$\frac{1}{R_L} = \frac{3}{2L} + \frac{\alpha^2}{\widehat{R}_L}, \tag{4.30}$$

with α and $\widehat{R}_L$ defined as

$$\alpha \equiv \frac{\sigma_s'}{\Sigma_s}, \tag{4.31}$$

$$\frac{1}{\widehat{R}_L} \equiv \frac{1}{R_L'} - \frac{3}{2L}. \tag{4.32}$$

The weight factors T_i with $i = 0, 1, 2$ are obtained as

$$T_0 = \frac{\delta^2}{\alpha^2} + h_1 \delta^2 \left(\frac{4L^2}{k^2}\right) Q(L), \tag{4.33}$$

$$T_1 = \frac{h_1 \alpha^2 \delta^2}{4} \left(1 - \frac{16L^4 Q^2(L)}{\widehat{R}_L^2 k^2}\right) - \left(\frac{2\delta^2 L^2}{R_L' \widehat{R}_L}\right) Q(L) - h_2 \left(\frac{\delta^2}{\alpha^2}\right) + i \left(\frac{k\delta^2}{2}\right) \left[\frac{1}{R_L'} + \left(\frac{h_1 \alpha^2}{\widehat{R}_L}\right) \left(\frac{4L^2}{k^2}\right) Q(L)\right], \tag{4.34}$$

$$T_2 = \frac{h_1 \alpha^2 \delta^2}{4} \left(1 + \frac{16L^4 Q^2(L)}{\widehat{R}_L^2 k^2}\right) + \left(\frac{2\delta^2 L^2}{R_L' \widehat{R}_L}\right) Q(L) + h_2 \left(\frac{\delta^2}{\alpha^2}\right) + \frac{1}{2} \ , \tag{4.35}$$

with

$$h_1 \equiv \frac{1}{\delta^2} - \frac{1}{\sigma_s'^2}, \tag{4.36}$$

$$h_2 \equiv \frac{1}{4\delta^2} + \frac{1}{4\sigma_s'^2} + \frac{1}{2\sigma_g'^2}. \tag{4.37}$$

The CSD in turbulence given in Eq. (4.27) recovers the CSD in free space expressed in Eq. (4.19) in the limit of $Q(L) \to 0$, which results in $\alpha = 1$. It is to be noted that the cross-spectral density in turbulence again has a very similar form to the propagated cross-spectral density in free space.

4.4.4 OAM spectrum of Rankine vortex beams

Having the cross-spectral density characterized in both free space and turbulence, we can now calculate the OAM spectrum for each case and evaluate the turbulence resistance.

Starting with the free space case, we substitute the CSD of Eq. (4.12) into the

angular integrals of Eq. (4.3); the mode intensity $I_m(\rho)$ can be expressed in the form

$$\begin{aligned} I_m(\rho) &= \left(\frac{\beta_0^4}{\delta^4}\right) \exp\left[-\left(\frac{1}{\sigma_s^2}+\frac{1}{\sigma_g^2}\right)\rho^2\right] \\ &\times \left\{\left[\delta^2 + 2\Re(S_1)\rho^2\right]\mathcal{I}_m\left(\frac{\rho^2}{\sigma_g^2}\right) + S_2\rho^2\mathcal{I}_{m-1}\left(\frac{\rho^2}{\sigma_g^2}\right)(S_2-1)\,\rho^2\mathcal{I}_{m+1}\left(\frac{\rho^2}{\sigma_g^2}\right)\right\}, \end{aligned} \tag{4.38}$$

where $\mathcal{I}_m$ is the modified Bessel function of order m and $\Re$ represents the real part.

To determine the overall OAM spectrum in the beam, it is necessary to integrate across the entire detector aperture, as in Eq. (4.4). In this manuscript, this radial integral will be evaluated numerically.

Given that the propagation in free space does not alter the distribution of energy among different OAM modes, we can affirm that the OAM spectrum of the source, as derived from Eq. (4.38), can be treated as the OAM spectrum detected in free space as well, provided we consider an infinite aperture, i.e. $R_d \to \infty$.

Following similar calculation steps, the OAM mode distribution at a radial distance r on propagation through turbulence takes the form,

$$\begin{aligned} I_m(r;L) &= \left(\frac{\beta_L^4}{\delta^4}\right)\left(\frac{w_0^4}{w_L^4}\right)\alpha^4 \exp\left[-\left(\frac{1}{\Sigma_s^2}+\frac{1}{\Sigma_g^2}\right)r^2\right] \\ &\times \left\{\left[T_0 + 2\Re(T_1)r^2\right]\mathcal{I}_m\left(\frac{r^2}{\Sigma_g^2}\right) + T_2 r^2\mathcal{I}_{m-1}\left(\frac{r^2}{\Sigma_g^2}\right) + (T_2-1)\,r^2\mathcal{I}_{m+1}\left(\frac{r^2}{\Sigma_g^2}\right)\right\}. \end{aligned} \tag{4.39}$$

We consider the case of an infinite aperture in Eq. (4.4), so that $R_d \to \infty$.

Figure (2) displays the resulting OAM spectrum in free space and turbulence for illustrative coherence widths of the Rankine vortex source. The beam is propagated 1 km through a turbulent media with the strength $C_n^2 = 10^{-14}$ m$^{-2/3}$. It can be seen that, as spatial coherence decreases, the two spectra become increasingly similar, suggesting that the beam OAM spectrum is less affected by turbulence. However, the mode spectrum for $\sigma_g = 0.5$ cm is overall much wider than the more coherent

$\sigma_g = 2$ cm case, indicating that this resistance is a pyrrhic victory. This seemed like the most likely outcome at the beginning of these studies, considering the mode spectrum of a partially coherent Rankine vortex is much wider than that of a coherent vortex. There is still the possibility that a Rankin vortex beam has its OAM spectrum spread more slowly than a coherent beam, and we will see that this is the case in Section 4.7.

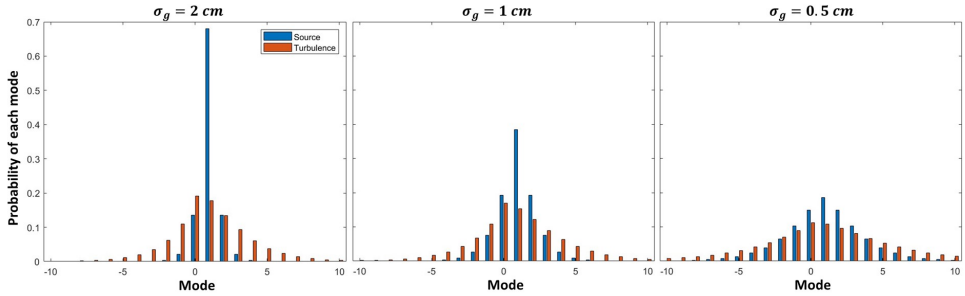

Figure 4.2: OAM spectrum of Rankine vortex beam at the source and in $L = 1000$ m propagation through turbulence with the strength $C_n^2 = 10^{-14}$ m$^{-2/3}$ for various coherence widths $\sigma_g = 0.5, 1, 2$ cm measured on an infinitely sized detector with $R_d \to \infty$. The beam size at the source is $\sigma_s = 1$ cm with the wavelength $\lambda = 632$ nm.

4.5 Twisted Gaussian-Schell Model Beams

Twisted Gaussian-Schell model (tGSM) beams, first introduced by Simon and Mukunda in 1993 [28], are modifications of the standard Gaussian-Schell model beams in which a phase twist is introduced into the state of coherence. In this type of partially coherent beam, the twist phase gives a handedness to the beam, which in turn results in a non-zero OAM for the beam. A tGSM source is characterized by the CSD,

$$W_0(\boldsymbol{\rho}_1, \boldsymbol{\rho}_2) = \exp\left(-\frac{\rho_1^2 + \rho_2^2}{2\sigma_s^2}\right) \exp\left(-\frac{|\boldsymbol{\rho}_1 - \boldsymbol{\rho}_2|^2}{2\sigma_g^2}\right) \exp\left[-iku(\boldsymbol{\rho}_1 \times \boldsymbol{\rho}_2) \cdot \hat{z}\right], \quad (4.40)$$

where σ_s and σ_g represent the beam size and coherence width at the source, respectively, and u is the twist parameter, whose sign characterizes the handedness and whose magnitude characterizes the strength of the twist, which is constrained to the

values

$$|u| \leq \frac{1}{k\sigma_g^2}, \tag{4.41}$$

and $\hat{z}$ is the unit vector in the direction of propagation.

4.5.1 Twisted GSM beams in free space

Propagation of tGSM beams in free space is obtained by evaluating Eq. (4.18) when the source is given by Eq. (4.40). The resulting CSD at the detector plane, located at distance L, is determined as

$$\begin{aligned} W_{\text{FS}}(\mathbf{r}_1', \mathbf{r}_2'; L) = A \exp\left(-\frac{r_1'^2 + r_2'^2}{2\sigma_s'^2}\right) \exp\left(-\frac{|\mathbf{r}_1' - \mathbf{r}_2'|^2}{2\sigma_g'^2}\right) \\ \times \exp\left[-iku_L'(\mathbf{r}_1' \times \mathbf{r}_2') \cdot \hat{\mathbf{z}}\right] \exp\left[-\frac{ik}{2R_L'}(r_1'^2 - r_2'^2)\right], \end{aligned} \tag{4.42}$$

where $\mathbf{r}_1'$ and $\mathbf{r}_2'$ are position vectors on the output plane. The parameters σ_s' , σ_g' , u_L' and R_L' are respectively the beam size, coherence width, twist parameter and the average radius of curvature in free space propagation, given by

$$\sigma_s'^2 = \frac{\sigma_s^2}{A}, \tag{4.43}$$

$$\frac{1}{2\sigma_g'^2} = \frac{A}{2\sigma_g^2}, \tag{4.44}$$

$$u_L' = Au, \tag{4.45}$$

$$R_L' = \frac{L}{1 - A}. \tag{4.46}$$

The parameter A is defined as

$$\frac{1}{A} \equiv 1 + \frac{L^2}{k^2}\left(\frac{1}{\sigma_s^4} + \frac{2}{\sigma_g^2\sigma_s^2} + k^2u^2\right). \tag{4.47}$$

As in the Rankine vortex case, we note that the propagated CSD has the same mathematical structure as the source CSD.

4.5.2 Twisted GSM beams in turbulence

Substituting the correlation function of the tGSM source given by Eq. (4.40) into the extended Huygens-Fresnel integral of Eq. (4.5) gives the CSD function of the tGSM beam at the detector plane in the form

$$W_{\text{T}}(\mathbf{r}_1, \mathbf{r}_2; L) = A\alpha^2 \exp\left(-\frac{r_1^2 + r_2^2}{2\Sigma_s^2}\right) \exp\left(-\frac{|\mathbf{r}_1 - \mathbf{r}_2|^2}{2\Sigma_g^2}\right) \times \exp\left[-ikU_L(\mathbf{r}_1 \times \mathbf{r}_2)\cdot\hat{z}\right] \exp\left[-\frac{ik}{2R_L}(r_1^2 - r_2^2)\right], \tag{4.48}$$

where $\mathbf{r}_1$ and $\mathbf{r}_2$ are the position vectors in the detector plane. The spot size Σ_s and radius of curvature R_L parameters for the beam in turbulence are determined using the expressions from Eq. (4.28) and Eq. (4.30). The quantities Σ_g and U_L are respectively the coherence width and twist parameters in turbulence, given by

$$\begin{aligned} \frac{1}{2\Sigma_g^2} =& \frac{1}{2\sigma_g'^2} + \frac{1}{4\sigma_s'^2} - \frac{1}{4\Sigma_s^2} + \left(\frac{3}{4} + \frac{\alpha^2 L^2}{\widehat{R}_L^2} + \alpha^2 L^2 u_L'^2\right) Q(L), \\ U_L =& \alpha^2 u_L', \end{aligned} \tag{4.49}$$

where the parameters α and $\widehat{R}_L$ are defined in Eqs. (4.31) and (4.32). As in the Rankine model case, the CSD function of tGSM beams in turbulence, as given in Eq. (4.48), converges to the free space result of Eq. (4.42) in the limit $Q(L) \to 0$, resulting in $\alpha = 1$.

4.5.3 OAM spectrum of tGSM beam

To analytically evaluate the OAM spectrum of the tGSM beam, we represent the twist phase term by a Bessel series representation (see [29], Sec.16.3),

$$\exp\left[-iku(\boldsymbol{\rho}_1 \times \boldsymbol{\rho}_2)\cdot\hat{z}\right] = \sum_{n=-\infty}^{\infty} \mathcal{J}_n(ku\rho_1\rho_2) e^{in(\phi_1 - \phi_2)}, \tag{4.50}$$

where again ρ and ϕ are the radial and azimuthal coordinates of position vector $\boldsymbol{\rho}$, respectively, and $\mathcal{J}_n$ represents the Bessel function of order n.

By applying the above relation in the expressions of tGSM beams at the source and in turbulence, we can characterize the intensity of each OAM mode on concentric circles in the beam cross-section through analytical calculations.

By substituting from Eq. (4.40) into Eq. (4.3) and evaluating the azimuthal integrals, the intensity of the OAM mode of order m at the radial distance ρ from the beam axis in the source plane is given as

$$I_m(\rho) = \sum_{n=-\infty}^{\infty} \exp\left[-\left(\frac{1}{\sigma_s^2} + \frac{1}{\sigma_g^2}\right)\rho^2\right] \mathcal{J}_n(ku\rho^2)\mathcal{I}_{n-m}\left(\frac{\rho^2}{\sigma_g^2}\right). \tag{4.51}$$

Again, since the OAM spectrum is preserved in free space propagation, the above result can be utilized to describe the OAM spectrum of the beam in free space propagation as well.

The distribution of intensity among OAM modes due to propagation through turbulence can be found by substituting from Eq. (4.48) into Eq. (4.3). The resulting expression is of the form

$$I_m(r; L) = \sum_{n=-\infty}^{\infty} \exp\left[-\left(\frac{1}{\Sigma_s^2} + \frac{1}{\Sigma_g^2}\right)r^2\right] \mathcal{J}_n(kU_L r^2)\mathcal{I}_{n-m}\left(\frac{r^2}{\Sigma_g^2}\right), \tag{4.52}$$

where r is the radial distance from the beam axis on the detector plane. The OAM spectrum for free space and turbulence can then be found by numerically evaluating the radial integral of Eq. (4.4).

Figure (3) illustrates the OAM spectrum on 1 km propagation through free space and turbulence for selected values of source coherence width σ_g. The twist magnitude was taken in each case to be the maximum allowed by Eq. (4.41), i.e. $u = 1/k\sigma_g^2$. In free space, we can see that the twist of the beam is represented by a mode spectrum skewed towards the positive modes. Analogous to the Rankine vortex case, we can see

that reducing the spatial coherence results in a greater resemblance between the free space and the turbulence mode spectrum, suggesting that the mode spectrum in this case is more resistant to turbulence. But as in the Rankine case, this comes at the cost of a significantly broadened mode spectrum to begin with, which indicates that tGSM beams will not necessarily alleviate cross-talk in OAM-based communications systems.

It is to be noted, however, that tGSM beams with low coherence do maintain their overall OAM spectra, as is evidenced by the skewness of the mode distribution being maintained. If a method can be found to discriminate tGSM beams by their twist parameter u, this twist parameter could potentially be a distinct method of encoding information in OAM-based communications. Currently, however, we are not aware of any method for doing such twist discrimination.

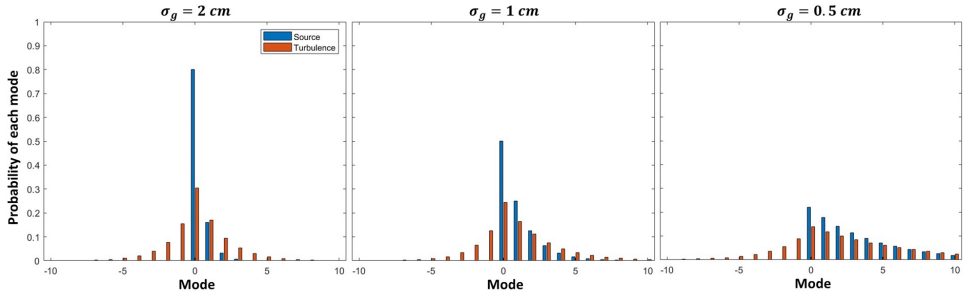

Figure 4.3: OAM spectrum of twisted Gaussian-Schell model beam with maximum possible twist magnitude $u = 1/k\sigma_g^2$ at the source and in propagation through turbulence (with the strength $C_n^2 = 10^{-14}$ m$^{-2/3}$) for various coherence widths $\sigma_g = 0.5, 1, 2$ cm. The beam size at source is $\sigma_s = 1$ cm, and the wavelength is $\lambda = 632$ nm. The propagation distance is $L = 1000$ m to an infinitely sized detector with $R_d \to \infty$.

4.6 Partially Coherent Beams with Circular Coherence

Circular coherence, introduced in 2017, describes a category of partially coherent sources that display perfect coherence along any ring concentric with the beam axis within the beam cross-section [12]. There is partial coherence between any two points on concentric rings with different radii, with coherence decreasing as the radial difference increases. The CSD function characterizing a circularly coherent beam (CCB)

may be expressed as

$$W_0(\boldsymbol{\rho}_1, \boldsymbol{\rho}_2) = U^*(\boldsymbol{\rho}_1)U(\boldsymbol{\rho}_2)g\left(\rho_1^2 - \rho_2^2\right). \tag{4.53}$$

Here, the average amplitude and phase is characterized by $U(\boldsymbol{\rho})$, while the degree of coherence is characterized by the function g, satisfying the condition $g(0) = 1$. A general partially coherent source can be defined by the method of Gori and Santarsiero [24],

$$W_0(\boldsymbol{\rho}_1, \boldsymbol{\rho}_2) = \int_{-\infty}^{\infty} H^*(\boldsymbol{\rho}_1, \nu)H(\boldsymbol{\rho}_2, \nu)P(\nu)d\nu, \tag{4.54}$$

where ν represents a beam parameter that varies in the statistical ensemble, possible multivariate, and $P(\nu)$ must be a non-negative Fourier transformable weight function so that the resulting CSD is physically realizable. It is to be noted that the beam wander model is a special case of this form.

Let us take the kernel $H(\boldsymbol{\rho}, \nu)$ to be a coherent field $U(\boldsymbol{\rho})$ with a finite radius of curvature [13],

$$H(\boldsymbol{\rho}, \nu) = U(\boldsymbol{\rho})e^{-2\pi i\nu\rho^2}, \tag{4.55}$$

which results in a ensemble of coherent beams that differ only in their curvature. These radii of curvature are determined as a function of the distribution variable ν as

$$R_0(\nu) = \frac{1}{2\lambda\nu}, \tag{4.56}$$

where λ is the wavelength. The resulting CSD can be expressed as

$$W_0(\boldsymbol{\rho}_1, \boldsymbol{\rho}_2) = U^*(\boldsymbol{\rho}_1)U(\boldsymbol{\rho}_2)\tilde{P}(\rho_1^2 - \rho_2^2), \tag{4.57}$$

where we have used the tilde symbol to represent the Fourier transform. This expression can be seen to directly relate to Eq. (4.53) defining circular coherence.

In this study, we have followed Santarsiero et al. [12] and taken the probability density to be of the form

$$P(\nu) = \Pi\left(\frac{\nu - \nu_0}{\Delta\nu}\right), \tag{4.58}$$

where $\Pi(\nu)$ indicates the rectangular function with value 1 for $|\nu| \leq 1/2$ and zero otherwise; this means that ν_0 and $\Delta\nu$ are respectively the center and width of the rectangular probability density.

In this case, if ν_0 is positive, the members of the ensemble will typically be focused, while negative ν_0 means the members will typically be defocused.

4.6.1 Circularly coherent vortex beams at source

We may introduce a circularly coherent beam (CCB) carrying OAM simply by choosing the coherent field $U(\boldsymbol{\rho})$ to be a vortex beam; curiously, this possibility has not yet been explored in detail [30]. Let us take the case of a first-order vortex,

$$U(\boldsymbol{\rho}) = \rho e^{i\phi} \exp\left(-\frac{\rho^2}{2\sigma_s^2}\right), \tag{4.59}$$

where σ_s represents the beam size. Upon substitution into Eq. (4.54), the CSD function takes the form,

$$\begin{aligned} W_0(\boldsymbol{\rho}_1, \boldsymbol{\rho}_2) = \int_{-\infty}^{\infty} \rho_1 \rho_2 e^{i(\phi_2 - \phi_1)} \exp\left[-\frac{1}{2\sigma_s^2}(\rho_1^2 + \rho_2^2)\right] \\ \times \exp\left[-2\pi i \nu(\rho_2^2 - \rho_1^2)\right] P(\nu) d\nu. \end{aligned} \tag{4.60}$$

4.6.2 Circularly coherent vortex beams in free space

By inserting the CCB source into the Huygens-Fresnel integral given in Eq. (4.18), the corresponding CSD function in free space is given as

$$W_{\text{FS}}(\mathbf{r}'_1, \mathbf{r}'_2; L) = \int_{-\infty}^{\infty} z_1'^{*} z'_2 \exp\left[-\frac{1}{2\sigma_s'^2(\nu)}\left(r_1'^2 + r_2'^2\right)\right] \times \exp\left[-\frac{ik}{2R'_L(\nu)}(r_1'^2 - r_2'^2)\right] P'(\nu)d\nu, \tag{4.61}$$

where z'_1 and z'_2 are the complex positions in the detector plane, located at distance L. Similar to the CSD at source, the above expression represents the CSD function at the detector plane by superimposing the coherent vortex beams with different sizes $\sigma'_s(\nu)$ and radii of curvature $R'_L(\nu)$, measured after propagation in free space. These parameters, dependent upon ν, are given by:

$$\sigma_s'^2(\nu) = \sigma_s^2 \left\{ \left[1 - \frac{L}{R_0(\nu)}\right]^2 + \left(\frac{L}{L_0}\right)^2 \right\}, \tag{4.62}$$

$$\frac{1}{R'_L(\nu)} = \frac{1}{L}\left\{1 - \left[\frac{\sigma_s}{\sigma'_s(\nu)}\right]^2 \left[1 - \frac{L}{R_0(\nu)}\right]\right\}, \tag{4.63}$$

where $L_0 = k\sigma_s^2$ is again the Rayleigh range for each of the coherent beams. The probability distribution function corresponding to the beam in free space undergoes a redefinition as

$$P'(\nu) = \left[\frac{\sigma_s}{\sigma'_s(\nu)}\right]^4 P(\nu). \tag{4.64}$$

4.6.3 Circularly coherent vortex beams in turbulence

Using the extended Huygens-Fresnel principle, the correlation function of CCB between the positions $\mathbf{r}_1$ and $\mathbf{r}_2$ at the detector plane after propagation through

turbulence can be written as

$$W_{\text{T}}(\mathbf{r}_1,\mathbf{r}_2;L)=\int_{-\infty}^{\infty}\left\{C_0(\nu)+C_1^*(\nu)r_1^2+C_1(\nu)r_2^2+C_2(\nu)z_1^*z_2+\left[C_2(\nu)-1\right]z_1z_2^*\right\}$$
$$\times\exp\left[-\frac{1}{2\Sigma_s^2(\nu)}\left(r_1^2+r_2^2\right)\right]\exp\left[-\frac{1}{2\Sigma_g^2(\nu)}|\mathbf{r}_1-\mathbf{r}_2|^2\right]$$
$$\times\exp\left[-\frac{ik}{2R_L(\nu)}(r_1^2-r_2^2)\right]\mathcal{P}(\nu)d\nu. \tag{4.65}$$

As is evident, turbulence effects give rise to a CSD function characterized by the superposition of Gaussian-Schell model vortex beams with different spot sizes $\Sigma_s(\nu)$, coherence widths $\Sigma_g(\nu)$ and radii of curvature $R_L(\nu)$, all defined as a function of probability variable ν with the following expressions,

$$\Sigma_s^2(\nu)=\sigma_s'^2(\nu)+Q(L)\left(\frac{4L^2}{k^2}\right), \tag{4.66}$$

$$\frac{1}{2\Sigma_g^2(\nu)}=\frac{1}{4\sigma_s'^2(\nu)}-\frac{1}{4\Sigma_s^2(\nu)}+Q(L)\left[\frac{3}{4}+\frac{L^2\,\alpha^2(\nu)}{\widehat{R}_L^2(\nu)}\right], \tag{4.67}$$

$$\frac{1}{R_L(\nu)}=\frac{3}{2L}+\frac{\alpha^2(\nu)}{\widehat{R}_L(\nu)}, \tag{4.68}$$

where the parameters $\alpha(\nu)$ and $\widehat{R}_L(\nu)$ were introduced in Eq. (4.31) and Eq. (4.32). The probability distribution function corresponding to the beam in turbulence is redefined as

$$\mathcal{P}(\nu)=\alpha^4(\nu)P'(\nu). \tag{4.69}$$

The relative weight factors C_i with $i = 0, 1, 2$ are introduced as

$$C_0(\nu) = Q(L)\left(\frac{4L^2}{k^2}\right), \tag{4.70}$$

$$C_1(\nu) = \frac{1}{4}\left[\alpha^2(\nu) - \frac{1}{\alpha^2(\nu)}\right] + Q^2(L)\left[\left(\frac{2L^2}{k}\right)\frac{\alpha(\nu)}{\widehat{R}_L(\nu)}\right]^2 + iQ(L)\left[\left(\frac{2L^2}{k}\right)\frac{\alpha^2(\nu)}{\widehat{R}_L(\nu)}\right], \tag{4.71}$$

$$C_2(\nu) = \frac{1}{4}\left[\alpha^2(\nu) + \frac{1}{\alpha^2(\nu)}\right] + Q^2(L)\left[\left(\frac{2L^2}{k}\right)\frac{\alpha(\nu)}{\widehat{R}_L(\nu)}\right]^2 + \frac{1}{2}. \tag{4.72}$$

The CSD function in turbulence, as expressed in Eq. (4.65), produces the free space result, given in Eq. (4.61), in the limit $Q(L) \to 0$, which indicates $\alpha = 1$.

4.6.4 OAM spectrum of circularly coherent vortex beam

From Eqs. (4.60) and (4.61), it is evident that the entire intensity of the circularly coherent vortex beam is concentrated in the OAM mode of order 1 at the source and in free space. The important question we will attempt to answer is whether a circularly coherent vortex beam performs better in turbulence – maintains a narrower mode spectrum – than a fully coherent vortex beam of the same order.

Due to the interaction with turbulent media, the power of the beam is distributed among higher-order modes. By substituting from Eq. (4.65) into Eq. (4.3) and evaluating the angular integrals, we get

$$I_m(r) = \int_{-\infty}^{\infty}\left\{\left[C_0(\nu) + 2\Re\left\{C_1(\nu)\right\}r^2\right]\mathcal{I}_m\left(\frac{r^2}{\Sigma_g^2}\right) + C_2(\nu)r^2\mathcal{I}_{m-1}\left(\frac{r^2}{\Sigma_g^2}\right) + \left[C_2(\nu) - 1\right]r^2\mathcal{I}_{m+1}\left(\frac{r^2}{\Sigma_g^2}\right)\right\}\exp\left[-\left(\frac{1}{\Sigma_s^2} + \frac{1}{\Sigma_g^2}\right)r^2\right]\mathcal{P}(\nu)\,d\nu, \tag{4.73}$$

where m is the order of the associated OAM mode. Unlike the Rankine and twisted cases, it is to be noted that it is not possible to get a closed form solution for $I_m(r)$ and

the integrals must be done computationally. Because of the self-focusing properties of the beams, they are not in general shape invariant on propagation, even in free space.

To explore the impact of transitioning from perfect coherence to partially circular coherence on resistance against turbulence effects, we compare the OAM spectrum of a fully coherent vortex beam with a flat phase front to that of a circularly coherent vortex beam; the results are in Fig. (4). The CCB is modeled by combining $N = 5$ beams with varying radii of curvature with values of ν equally spaced within the range of $(\nu_0 - \Delta\nu/2, \nu_0 + \Delta\nu/2)$, with $\Delta\nu = 0.001/\lambda L$. This combination is determined by the probability distribution function given in Eq. (4.58). As is evident from Figs. 4(a) and 4(c), the defocused beams with negative curvature display unfavorable effects, with a broader spectrum compared to the coherent case. Conversely, in Figs. 4(b) and 4(d), positive curvature provides advantages over the fully coherent beam.

Upon closer examination of Figs. 4(b) and 4(d), it is demonstrated that the radius of curvature $R_0 = L$, equivalent to $\nu_0 = 1/2\lambda L$, results in a spectrum profile with less spread and higher central peak, suggesting greater resistance against turbulence compared to the beam with a curvature $R_0 = 2L$, equivalent to $\nu_0 = 1/4\lambda L$.

From the results of Fig. (4), it can be concluded that transitioning to partially circular coherence does not always provide better resistance of the OAM spectrum on propagation through turbulence. Selecting a judicious value for the radius of curvature at the source is essential to optimize the generated beam for an effective turbulence propagation. We have discussed the circular coherence case in more detail in an upcoming publication [31].

In the upcoming section, we will compare the behavior of all three types of PCBs in interaction with atmospheric turbulence. This comparison will be facilitated by examining the standard deviation of their OAM spectrum profiles.

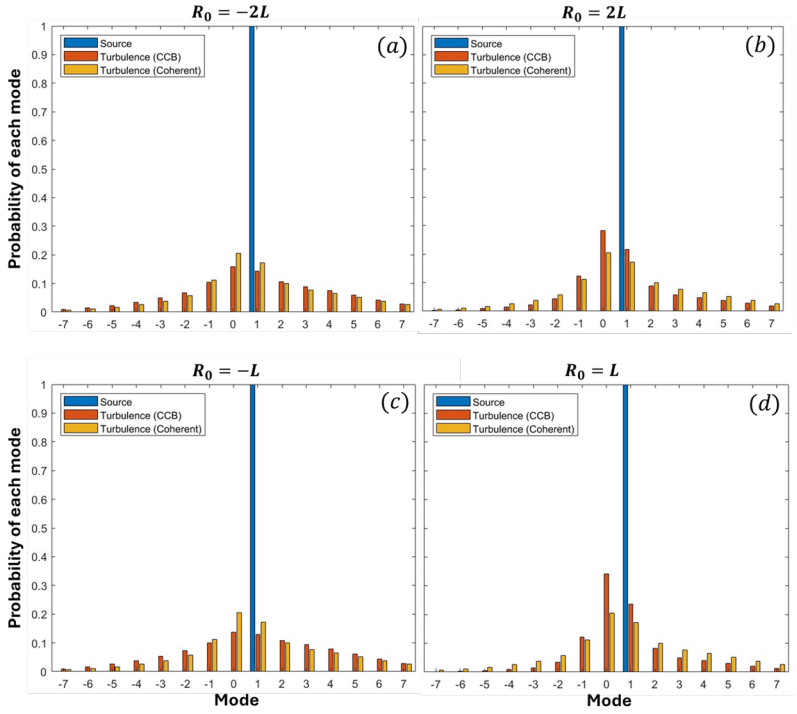

Figure 4.4: OAM spectrum of fully coherent and circularly coherent vortex beams for different central values of radius of curvature of the superimposed beams at source in $L = 1000$ m propagation through turbulence (with the strength $C_n^2 = 10^{-14}$ m$^{-2/3}$). The beam size at source is $\sigma_s = 1$ cm, and the wavelength is $\lambda = 632$ nm. The number of superimposed beams at source is $N = 5$.

4.7 Comparing the three PCB classes

After introducing the three classes of OAM-carrying partially coherent beams and delving into the propagation of their cross spectral density function through turbulence, as well as analyzing the behavior of their respective OAM spectra under turbulence disturbances individually, we now compare the resilience of the three beam types against the effects of turbulence.

We have noted that both the Rankine model beam and the CCB are produced by manipulating the parameters of a fully coherent Gaussian vortex source. In the Rankine model, the position of the coherent beam axis is randomized, whereas in the CCB, coherent beams with various radii of curvature are superimposed. In a tGSM beam, the initial source is a zero-order Gaussian beam without any OAM, and one can show that the OAM is induced by using an ensemble of beams that are all tilted to produce a net handedness [32].

In order to assess and compare the robustness of the OAM spectra for these beams, we consider the standard deviation of the OAM spectrum associated with each beam type; the standard deviation quantifies the dispersion of power among different OAM modes. A lower standard deviation indicates a narrower OAM spectrum, suggesting better mode purity in the face of turbulence and a beam that is more useful for OAM-based communications.

In Figure (5), a comparison is presented of the standard deviations associated with a fully coherent vortex beam, Rankine model vortex beam, twisted Gaussian-Schell model beam and partially coherent vortex beam with circular coherence. As is evident, for propagation distances less than about 250 m, the Rankine an tGSM beams have broader OAM spectra compared to the fully coherent case. In contrast, the CCB demonstrates a significantly narrower spectrum compared to a fully coherent beam.

As the distance surpasses 700 m, both the coherent beam and CCB exhibit a

notable rise in standard deviation. Meanwhile, the standard deviation profiles of the Rankine and tGSM beams exhibit a gentle slope, indicating consistent stability and greater resistance. Our initial hypothesis, mentioned at the end of Section 4.4, was that randomized partially coherent vortex beams might have a slower spread of their OAM spectra in turbulence, and this appears to be the case.

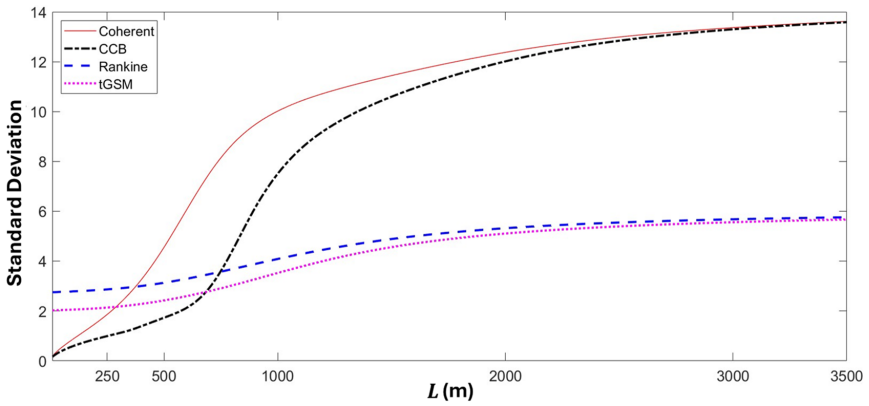

Figure 4.5: Standard deviations of the OAM spectra versus propagation distance through turbulence (with the strength $C_n^2 = 10^{-14}$ m$^{-2/3}$) corresponding to a fully coherent Gaussian vortex beam, Rankine model vortex beam, twisted Gaussian-Schell model beam and circularly coherent beam. The beam size at source is $\sigma_s = 1$ cm, and the wavelength is $\lambda = 632$ nm. Coherence width of the Rankine and tGSM model beam is $\sigma_g = 0.5$ cm. The CCB is comprised of $N = 5$ Gaussian vortex beams with various radii of curvature in the range $(\nu_0 - \Delta\nu/2, \nu_0 + \Delta\nu/2)$ with $\Delta\nu = 0.001/\lambda L$ and $\nu_0 = 3/4\lambda L$, equivalent to $R_0 = 2L/3$. The radius of the detector is $R_d = 1$ m.

4.8 Conclusion

We have conducted an analytic investigation into how reducing the coherence of an OAM-carrying beam affects its resistance to atmospheric turbulence. "Resistance," in this case, refers to how well the beam maintains its OAM purity on propagation through turbulence. We considered three physically distinct models of partially coherent OAM beams: Rankine model, twisted Gaussian-Schell model and circularly coherent beams. By examining an OAM beam corresponding to each class and deriving its mode spectrum after propagation through turbulence, we analyzed the advantages and disadvantages of coherence reduction associated with each class.

We use the standard deviation of the OAM spectrum to quantify the purity of the OAM state of the beam. The standard deviation is viewed as a basic metric for assessing the reliability of data transmission using OAM modes. A larger standard deviation suggests that data channels just be given wider OAM spacing in order to avoid crosstalk, which reduces the number of channels available.

The comparison of the standard deviations of the three types of PCBs and the coherent beam has indicated that for short propagation distances, the coherent beam and an optimized CCB have better performance of the four. However, over longer propagation distances, the OAM spectrum of coherent beam and CCB expand dramatically, leaving the Rankine and tGSM beams with narrower spectra. The advantages offered by the Rankine and tGSM beams become increasingly prominent over longer propagation distances; however, it should be noted that these beams have a significant standard deviation to begin with that may limit their usefulness.

Our results provide guidelines for further investigations into the propagation of partially coherent vortex beams in turbulence. It is possible to encode OAM in partially coherent beams in more sophisticated ways beyond the classes considered here, for instance by considering twisted vortex GSM beams [9] or beams with polarization singularities encoded [34]; these will provide avenues for future study.

REFERENCES

[1] Gibson, G. G., Courtial, J., Padgett, M. J., Vasnetsov, M., Pas ko, V., Barnett, S. M., and Franke-Arnold, S. (2004). Free-space information transfer using light beams carrying orbital angular momentum. Optics Express, 12(22), 5448-5456.

[2] Willner, A. E., Huang, H., Yan, Y., Ren, Y., Ahmed, N., Xie, G., ... & Ashrafi, S. (2015). Optical communications using orbital angular momentum beams. Advances in Optics and Photonics, 7, 66-106.

[3] Ricklin, J. C., & Davidson, F. M. (2002). Atmospheric turbulence effects on a partially coherent Gaussian beam: implications for free-space laser communication. Journal of the Optical Society of America A, 19(9), 1794-1802.

[4] Gbur, G., & Wolf, E. (2002). Spreading of partially coherent beams in random media. Journal of the Optical Society of America A, 19(9).

[5] Korotkova, O., Andrews, L. C., & Phillips, R. L. (2004). Model for a partially coherent Gaussian beam in atmospheric turbulence with application in Lasercom. Optical Engineering, 43.

[6] Gbur, G. (2018). Partially coherent vortex beams. In Proceedings of SPIE (Vol. 10549) (p. 1054903).

[7] Swartzlander, G., & Hernandez-Aranda, R. (2007). Optical Rankine Vortex and Anomalous Circulation of Light. Physical Review Letters, 99, 163901.

[8] Kim, S. M., & Gbur, G. (2009). Momentum conservation in partially coherent wave fields. Physical Review A, 79, 033844.

[9] Stahl, C. S. D., & Gbur, G. (2017). Partially coherent vortex beams of arbitrary order. Journal of the Optical Society of America A, 34, 1793-1799.

[10] Hou, W., Liu, L., Liu, X., Cai, Y., & Peng, X. (2024). Statistical Properties of a Twisted Gaussian Schell-Model Beam Carrying the Cross Phase in a Turbulent Atmosphere. Photonics, 11(2), 124. https://doi.org/10.3390/photonics11020124.

[11] Bogatyryova, G. V., Fel de, C. V., Polyanskii, P. V., Ponomarenko, S. A., Soskin, M. S., & Wolf, E. (2003). Partially coherent vortex beams with a separable phase. Optics Letters, 28(11), 878-880.

[12] Santarsiero, M., MartÃnez-Herrero, R., Maluenda, D., de Sande, J. C. G., Piquero, G., & Gori, F. (2017). Partially coherent sources with circular coherence. Optics Letters, 42(8), 1512-1515.

[13] Ding, C., Koivurova, M., Turunen, J., & Pan, L. (2017). Self-focusing of a partially coherent beam with circular coherence. Journal of the Optical Society of America A, 34(8), 1441-1447.

[14] Wolf, E. (1982). New theory of partial coherence in the space frequency domain. Part I: spectra and cross spectra of steady-state sources. Journal of the Optical Society of America, 72(3), 343 351.

[15] Korotkova, O., & Gbur, G. (2021). Unified matrix representation for spin and orbital angular momentum in partially coherent beams. Physical Review A, 103, 023529.

[16] Allen, L., Beijersbergen, M., Spreeuw, R., abd Woerdman, J. (1992). Orbital angular momentum of light and the transformation of Laguerre Gaussian laser modes. Physical Review A, 45, 8185-8189

[17] Mirhosseini, M., Malik, M., Shi, Z., & Boyd, R. W. (2013). Efficient separation of the orbital angular momentum eigenstates of light. Nature Communications, 4, 2781.

[18] Korotkova, O., and Gbur, G. (2021). Jones and Stokes Mueller analogous calculi for OAM-transforming optics. Optics Letters, 46, 2585 2588.

[19] Lutomirski, R., & Yura, H. (1971). Propagation of a finite optical beam in an inhomogeneous medium. Applied Optics, 10, 1652-1658.

[20] Gbur, G. (2014). Partially coherent beam propagation in atmospheric turbulence [Invited]. Journal of the Optical Society of America A, 31, 2038-2045.

[21] Lin, S., Wang, C., Zhu, X., Lin, R., Wang, F., Gbur, G., ... and Yu, J. (2020). Propagation of radially polarized Hermite non uniformly correlated beams in a turbulent atmosphere. Optics Express, 28, 27238 27249.

[22] Andrews, L. C., & Phillips, R. L. (2005). Laser Beam Propagation through Random Media. SPIE.

[23] Shiri, A., Schmidt, J., Tellez, J., and Gbur, G. (2023). Modified Huygens Fresnel method for the propagation of partially coherent beams through turbulence. Journal of the Optical Society of America A, 40, 470 478.

[24] Gori, F., & Santarsiero, M. (2007). Devising genuine spatial correlation functions. Optics Letters, 32, 3531-3533.

[25] Gbur, G., Visser, T. D., & Wolf, E. (2004). "'Hidden' singularities in partially coherent wavefields." Journal of Optics A: Pure and Applied Optics, 6(Suppl.), S239.

[26] Gbur, G. J. (2017). Singular Optics. CRC Press.

[27] Gradshteyn, I. S., & Ryzhik, I. M. (2007). Table of Integrals, Series, and Products (7th ed.). Academic Press.

[28] Simon, R., & Mukunda, N. (1993). Twisted Gaussian Schell-model beams. Journal of the Optical Society of America A, 10, 95-109.

[29] Gbur, G. J. (2011). Mathematical Methods for Optical Physics and Engineering. Cambridge University Press.

[30] R. Qi, A. Shiri and G. Gbur, Circularly coherent vortex beams, in preparation.

[31] A. Shiri, R. Qi and G. Gbur, Circularly coherent vortex beams optimized for propagation through turbulence, submitted.

[32] D. Ambrosini , V. Bagini , F. Gori and M. Santarsiero (1994) Twisted Gaussian Schell-model Beams: A Superposition Model, Journal of Modern Optics, 41:7, 1391-1399.

[33] C.S.D. Stahl and G. Gbur, Twisted vortex Gaussian Schell-model beams, J. Opt. Soc. Am. A 35 (2018), 1899.

[34] J. Mays and G. Gbur, Angular momentum of vector-twisted-vortex Gaussian Schell-model beams, J. Opt. Soc. Am. A 40 (2023), 1417-1424.

CHAPTER 5: CONCLUSIONS

5.1 Summary

This dissertation investigated a potential method to improve the reliability of data transmission channels in OAM-based free space optical communication systems. The proposed method was grounded in the principle that reducing coherence results in increased resistance of light beams to atmospheric turbulence influences. On the other hand, decreasing coherence leads to an increase in cross-talk between adjacent channel modes. The main objective was identifying a type of partially coherent beam in which the advantages of coherence reduction outweigh its disadvantages.

Chapter 2 introduced a novel analytical approach for propagation of partially coherent beams through turbulence by modifying the traditional extended Huygens-Fresnel principle. As a result, the four-fold integral of the eHF principle was simplified to a two-fold integral, which makes both the analytical and computational evaluation of the cross spectral density function feasible. In this approach, the turbulence effects were represented as a distortion of the beam detected at the detector after propagation through vacuum. In our model, the binomial approximation for the turbulence complex phase was considered. Additionally, two criteria were introduced to estimate the propagation distance over which the intensity and coherence of the light field remain unchanged under the influence of turbulence. At the end, propagation of the Gaussian-Schell model beam was evaluated as an example to validate the correctness of the modified Huygens-Fresnel method and assess accuracy of the criteria for turbulence resistance estimates.

In chapter 3, we analyzed the behavior of a class of separable phase PCB in interaction with atmospheric turbulence. This specific type of beam with pure OAM state

at its source, known as circularly coherent vortex beam, can be generated through linear combination of coherent beams with varying radii of curvature. The study revealed that the circularly coherent vortex beams can be optimized to exhibit enhanced resistance to turbulence compared to its coherent counterpart. In the optimization process, we introduced a parameter, denoted as Ω, defined as the ratio of correlation width to beam size of the detected field. This parameter can serve as an indicator for determining the optimal choice of partially coherent beams for propagating through turbulence. For the circularly coherent vortex beams, this parameter is predominantly determined by the average wavefront curvature of the constituent beams and is minimally impacted by the spatial coherence of the generated field. The findings underscore a phenomenon of turbulence propagation termed as "beamlet diversity", wherein the individual beamlets comprising a partially coherent beam need to exhibit significant dissimilarity from one another to enhance the beam's resilience against turbulence. For circularly coherent vortex beams, the radii of curvature of beamlets must fall within a relatively narrow range, implying that only a few beamlets are needed to satisfy the requirements for beam generation at its source. This condition limits the variation of beamlets and, consequently, restricts the potential for enhancing resistance

In Chapter 4, the turbulence propagation of three fundamental classes of partially coherent beams has been evaluated analytically, and the behavior of their respective OAM spectra has been investigated in detail. The standard deviation of OAM spectrum has been introduced as a measure of the robustness of an OAM-based data transmission system, implying that beams with more stable OAM spectra exhibit lower standard deviation when propagating through turbulence. It is demonstrated that, in short propagation distances, improving the reliability of data transmission through reducing coherence can be achieved only for the case of partially coherent beams with circular coherence. For the other types of PCBs, the Rankine vortex and

twisted Gaussian-Schell model beams, reducing coherence brings about higher cross-talk between data channels. Conversely, along with the extension of propagation to longer distances, OAM spectra of the pre-randomized Rankine model and tGSM beams exhibit higher stability than the coherent beams and CCBs.

5.2 Future Works

The research done suggests several promising areas for future research including:

1. Investigating other types of OAM-carrying PCBs in search of more robust OAM spectra in propagation through atmospheric turbulence.

2. By conducting calculations of the intensity correlations of PCBs, one can gain insights into properties such as the scintillation of the beams in turbulence and the bit-error rate of free-space optical communication systems [11].

3. Given the established resistance of circularly coherent beams against turbulence, exploring other classes of PCBs with circular coherence may unveil even greater advantages compared to the beam types studied thus far [12].

4. Other characteristic features of light may show higher stability in propagation in both free space and turbulence, such as topological structures. Exploring these properties as data carriers in optical communication systems has the potential to further enhance data capacity while ensuring higher reliability [13].

REFERENCES

[1] O.V. Angelsky, A.Y. Bekshaev, S.G. Hanson, C.Y. Zenkova, I.I. Mokhun, and J. Zheng, "Structured Light: Ideas and Concepts," Front. Phys. 8:114 (2020).

[2] Ritsch-Marte M. Orbital angular momentum light in microscopy. Philos Trans A Math Phys Eng Sci. 2017 Feb 28;375(2087):20150437. doi: 10.1098/rsta.2015.0437. PMID: 28069768; PMCID: PMC5247481

[3] Fu, S., Zhai, Y., Zhang, J. et al. Universal orbital angular momentum spectrum analyzer for beams. PhotoniX 1, 19 (2020). https://doi.org/10.1186/s43074-020-00019-5

[4] Graham Gibson, Johannes Courtial, Miles J. Padgett, Mikhail Vasnetsov, Valeriy Pasko, Stephen M. Barnett, and Sonja Franke Arnold, "Free space information transfer using light beams carrying orbital angular momentum," Opt. Express 12, 5448 5456 (2004)

[5] A. E. Willner, H. Huang, Y. Yan, Y. Ren, N. Ahmed, G. Xie, C. Bao, L. Li, Y. Cao, Z. Zhao, J. Wang, M. P. J. Lavery, M. Tur, S. Ramachandran, A. F. Molisch, N. Ashrafi, and S. Ashrafi, "Optical communications using orbital angular momentum beams," Adv. Opt. Photon. 7, 66-106 (2015)

[6] Jennifer C. Ricklin and Frederic M. Davidson, Atmospheric turbulence effects on a partially coherent Gaussian beam: implications for free-space laser communication, J. Opt. Soc. Am. A 19, 1794-1802 (2002).

[7] G. Gbur and E. Wolf, Spreading of partially coherent beams in random media, J. Opt. Soc. Am. A 19 (2002).

[8] Olga Korotkova, Larry C. Andrews, Ronald L. Phillips, "Model for a partially coherent Gaussian beam in atmospheric turbulence with application in Lasercom," Opt. Eng. 43 (2004),

[9] J. M. Martin and Stanley M. Flatté, "Intensity images and statistics from numerical simulation of wave propagation in 3-D random media," Appl. Opt. 27, 2111-2126 (1988).

[10] L. C. Andrews and R. L. Phillips, "Laser Beam Propagation through Random Media" (SPIE, 2005)

[11] Josselin Garnier and Knut SÃžlna, "Scintillation of partially coherent light in time-varying complex media," J. Opt. Soc. Am. A 39, 1309-1322 (2022)

[12] MartÃnez-Herrero R, Santarsiero M, Piquero G, GonzÃ¡lez de Sande JC. A New Type of Shape-Invariant Beams with Structured Coherence: Laguerre-Christoffel-Darboux Beams. Photonics. 2021; 8(4):134. https://doi.org/10.3390/photonics8040134

[13] Won, R. Shaping the topology of light. Nature Photon 8, 8 (2014). https://doi.org/10.1038/nphoton.2013.358